

REACTIVE REJUVENATION OF CMOS LOGIC PATHS  
USING SELF-ACTIVATING VOLTAGE DOMAINS

by

NAVID KHOSHAVI NAJAFABADI  
M.S. Amirkabir University of Technology 2012

A thesis submitted in partial fulfillment of the requirements  
for the degree of Master of Science  
in the Department of Electrical and Computer Engineering  
in the College of Engineering and Computer Science  
at the University of Central Florida  
Orlando, Florida

Summer Term  
2016

Major Professor: Ronald F. DeMara

© 2016 Navid Khoshavi Najafabadi

## ABSTRACT

Aggressive CMOS technology scaling trends exacerbate the aging-related degradation of propagation delay and energy efficiency in nanoscale designs. Recently, power-gating has been utilized as an effective low-power design technique which has also been shown to alleviate some aging impacts. However, the use of MOSFETs to realize power-gated designs will also encounter aging-induced degradations in the sleep transistors themselves which necessitates the exploration of design strategies to utilize power-gating effectively to mitigate aging. In particular, Bias Temperature Instability (BTI) which occurs during activation of power-gated voltage islands is investigated with respect to the placement of the sleep transistor in the header or footer as well as the impact of ungated input transitions on interfacial trapping. Results indicate the effectiveness of power-gating on NBTI/PBTI phenomena and propose a preferred sleep transistor configuration for maximizing higher recovery.

Furthermore, the aging effect can manifest itself as timing error on critical speed-paths of the circuit, if a large design guardband is not reserved. To mitigate circuit from BTI-induced aging, the Reactive Rejuvenation (RR) architectural approach is proposed which entails detection and recovery phases. The BTI impact on the critical and near critical paths performance is continuously examined through a lightweight logic circuit which asserts an error signal in the case of any timing violation in those paths. By observing the timing violation occurrence in the system, the timing-sensitive portion of the circuit is recovered from BTI through switching computations to redundant aging-critical voltage domain. The proposed technique achieves aging mitigation and reduced energy consumption as compared to a baseline circuit. Thus, significant

voltage guardbands to meet the desired timing specification are avoided result in energy savings during circuit operation.

*I dedicate my thesis work to my family and many friends. A special feeling of gratitude to my wife, Sahar who never left my side throughout the entire my Master program. A special feeling of thankful to my parents whose unlimited support either financially or intellectually made this thesis possible. I dedicate this work and special thanks to not only my advisor, but also one of my friends for sharing his knowledge about how I can become a successful researcher.*

## **ACKNOWLEDGMENTS**

I owe my gratitude to many people who made this thesis possible even only my name will be appeared on the cover of this thesis. I have been amazingly fortunate to work under supervision of Dr. DeMara who patiently supported me even in tough situations and continuously motivated me to become a successful student. His insightful comments and immense knowledge helped me to shape my ideas at different stage of my research which leads to publishing several papers in the well-known conferences. I would like to extend special thanks to Dr. Jiann Yuan and Dr. Zixia Song for serving in my thesis committee. A special thanks to Rizwan Ashraf for helping me with the tools and proof reading my papers.

## TABLE OF CONTENTS

LIST OF FIGURES .....	x
LIST OF TABLES .....	xii
CHAPTER ONE: INTRODUCTION.....	1
Need for Reliability Strategies in Highly Scaled CMOS Circuits.....	1
Transient Faults.....	2
Permanent Faults.....	3
Degradation Effects .....	4
The BTI Phenomenon .....	5
The NBTI Process and its Impact on the Circuit's Lifetime .....	6
The PBTI Process and its Impact on the Circuit's Lifetime .....	8
The BTI Physics and Aging Model .....	8
Categories of BTI Mitigation Methods.....	10
Contribution of Thesis .....	11
Organization of Thesis .....	13
CHAPTER TWO: THE AGING PREDICTION TECHNIQUES .....	14
CHAPTER THREE: THE AGING MEASUREMENT TECHNIQUES .....	19
CHAPTER FOUR: THE AGING MITIGATION TECHNIQUES.....	23
Worst-case Design Techniques for Aging-Compensation.....	24

Voltage-Margin (VM).....	24
Gate-Sizing .....	26
Dynamic Operating Conditions for Aging-Mitigation .....	27
Dynamic Voltage and/or Frequency Scaling .....	27
Computational Sprinting.....	28
Adaptive Resource Management for Aging-Resilience .....	29
Idle-Time Leveraging (ITL) Schemes .....	29
Controlled Resource Wearout to Improve Performance.....	31
Structural Duplication (SD) .....	31
Logic-Wear-Leveling (LWL) .....	32
Reactive Rejuvenation (RR) .....	32
Summary .....	33
 CHAPTER FIVE: POWER-GATING STRATEGIES FOR AGING MITIGATION OF CMOS	
LOGIC PATHS.....	35
Power-Gating Scenarios.....	36
Experimental Results .....	39
$V_{th}$ Shift.....	40
Delay Penalty .....	41
Input Vector Impact on BTI Recovery .....	44
Analysis and Conclusion.....	44



CHAPTER SIX: REACTIVE REJUVENATION OF CMOS LOGIC PATHS USING SELF- ACTIVATING VOLTAGE DOMAINS .....	47
Bti-Induced Aging Rejuvenation of Aging-critical Logic .....	47
Aging-aware Dispatcher for Representative Aging-critical Logic Selection .....	48
Remodeling Aging-critical Logic .....	50
Experimental Results .....	50
Critical Path Remodeling Tool (CPRT).....	52
RR Reduction of Delay Degradation .....	53
RR Area Overhead.....	54
CHAPTER SEVEN: CONCLUSION .....	57
Technical Summary .....	57
Trading Area for Energy .....	59
Technical Insights Gained.....	60
Future Works .....	61
APPENDIX A: HSPICE CODE FOR BASIC INVERTER CHAIN RELIABILITY ASSESSMENT .....	62
APPENDIX B: HSPICE CODE FOR INVERTER CHAIN WITH FOOTER SLEEP TRANSISTOR RELIABILITY ASSESSMENT .....	65
APPENDIX C: HSPICE CODE FOR I5 BENCHMARK IN RR METHOD .....	71
REFERENCES .....	78

## LIST OF FIGURES

Figure 1: The impact of ionizing particle in a reverse-biased p-n junction (based on [4]).....	2
Figure 2: Increasing failure ratio due to accelerated transistor aging (1) and vulnerability to soft errors (2) [12] [13]. .....	6
Figure 3: The NBTI stress and recovery illustration (based on [14] and [24]) .....	7
Figure 4: The PBTI stress and recovery illustration (based on [14] and [24]) . .....	7
Figure 5: Proactive vs. reactive techniques [12]. .....	10
Figure 6: Organization of Thesis .....	13
Figure 7: Taxonomy of aging mitigation techniques. ....	23
Figure 8: Sampling the output data at two different points in time [1].....	33
Figure 9: Autonomous aging-aware resource management for $N = 2$ [1, 12] .....	34
Figure 10: The original circuit .....	38
Figure 11: The Header-based ST circuit .....	38
Figure 12: The Footer-based ST circuit .....	38
Figure 13: The Header and Footer based ST circuit .....	38
Figure 14: Taxonomy of ST Arrangements and their characteristics .....	39
Figure 15: Comparison of increased $V_{th}$ for 100KHz signal .....	42
Figure 16: Comparison of increased $V_{th}$ for 1KHz signal .....	42
Figure 17: Comparison of increased $delay$ for 100KHz signal.....	43
Figure 18: Comparison of increased $delay$ for 1KHz signal.....	43
Figure 19: Comparison of $V_{th}$ shift for the first 3 NMOS of CUT.....	45
Figure 20: Comparison of $V_{th}$ shift for the first 3 PMOS of CUT .....	45

Figure 21: Timing diagram before aging [2, 3] .....	49
Figure 22: Timing diagram after aging [2] .....	49
Figure 23: Critical path replication. Here $CP^i$ denotes $i^{th}$ instance of the critical path.....	51
Figure 24: Operation of CPRT within EDA design flow [1]. .....	52
Figure 25: Normalized propagation delay of multiple aging-critical logic over time for c880 with ERT=2% using Uncompensated Design and RR schemes. ....	55
Figure 26: Percent energy savings relative to Baseline. ERT=1% and ERT=2% depicted for benchmark circuits. ....	55

## LIST OF TABLES

Table 1: Comparison of aging prediction techniques. ....	18
Table 2: Comparison of several aging sensors (as adapted from [41]).....	22
Table 3: Comparison of the aging mitigation techniques [46]. ....	25
Table 4: Delay degradation Comparison (% baseline) .....	46
Table 5: Power Consumption Comparison (in Watts).....	46
Table 6: The minimum switching intervals obtained by RR for ERT=1% and ERT=2% .....	56
Table 7: Initial Time Area/Energy Overheads with ( $n = 2$ ) at Nominal Voltage .....	56

## CHAPTER ONE: INTRODUCTION

The CMOS technology advancements over past decades has introduced more accurate and cost-efficient techniques for manufacturing the electronic devices. The demand for delivering greater performance in a smaller chip area has motivated the International Technology Roadmap for Semiconductors (ITRS) community to significantly investigate the challenges of entering the nanometer scale CMOS technology era [2]. Even though the CMOS technology scaling has provided the billions of transistors in a small-scale die area to elevate the performance of the system, this advancement has also augmented the reliability concerns in different abstraction stages from the architecture level to gate level.

### Need for Reliability Strategies in Highly Scaled CMOS Circuits

To enable the circuit designers to efficiently address the reliability issues associated with scaling down the transistor size, the source of these reliability exposures warrants investigation. Although research into the details of each reliability issue is out of scope of this thesis, we will briefly present some of the design-related aspects in the following subsections to facilitate generalization of the discussed approaches and to foster new inspiring techniques for this important reliability phenomenon leading to advancements in the design of defect-tolerant digital circuits.

## Transient Faults

*Transient faults* can be induced by impact of energetic particles that penetrate the silicon substrate and generate electron-hole pairs along their tracks as illustrated in Figure 1. If a single particle hits the logic circuit, it might result in a glitch or pulse in the transferred signal across combinational logic elements. This category of transient faults is known as *Single-Event Transient (SET)* [3]. On the other hand, if the memory cell state flips due to either the directly strike radiation particle or an SET, the occurred transient fault is referred as *soft error* or *Single-Event Upset* [3]. Over past years, the susceptibility of both combinational and sequential logics to soft errors has dramatically increased by reducing the transistor's footprint size, operating voltage, and guardbanding [3].

In order to clarify how the transient faults may effect on the circuit's output, we have briefly demonstrated this phenomenon as the following. It begins with the collection of the generated electron-hole pairs due to transient fault in the pn junction through the so-called funneling mechanism as shown in Figure 1. While the most of released charges are absorbed in the struck junction, the remained charges are diffused into the substrate.

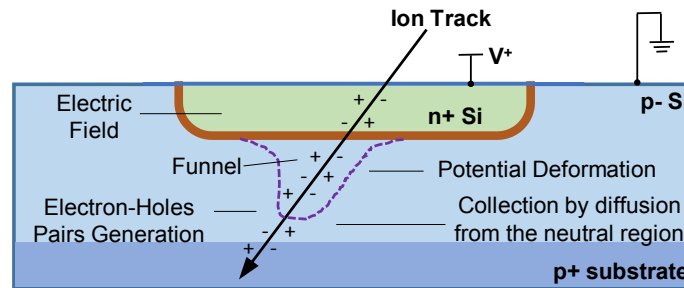


Figure 1: The impact of ionizing particle in a reverse-biased p-n junction (based on [4]).

In particular, if these impinging charges are collected by a sensitive node such as the reverse biased drain pn junction, it may change the amount of the potential at the drain node and lead to flipping of the initial state if it is captured by a flip-flop [5] [6]. In addition, by further reducing the critical charge and the distance between junctions with scaling, the probability of affecting a single low-energy radiation particle on the output of multiple circuit nodes has significantly increased. It is anticipated that this trend will continue as long as the technology scaling occurs and even will get worse by introducing aggressive voltage drop for larger energy saving in the low-power circuit designs [4]. Thus, the low-power fault-tolerant circuit and system designs have received significant attention over past years to overcome the scaling challenges through cost-effective, low-power and high performance fault detection and management mechanism.

### Permanent Faults

Permanent faults are referred to those faults that have continuous impact on the circuit's function and may cause the wrong results in the output. Since the permanent faults would not be vanished prior the entire replacement of defected component, the test technique can be executed repeatedly to find the erroneous counterpart while it is expected to observe identical results for all test iterations. Permanent faults are often the consequence of a malfunction in the manufacturing process. In other words, if the hardware design differentiates from its implementation, the unintended difference has the potential to impact the circuit's output. These faults may eventually result in the circuit failure such as opens, shorts, leakage, and threshold voltage shift [7] [8].

The probability of circuit failure has increased proportionally with the level of technology scaling. The main reason is that more transistors can be integrated into the same-sized chip by downscaling the circuit feature which in turn cause the proportional increase of failure in the nanoscale circuits. For example, the doping profile fluctuation can result in high deviation of the transistor threshold voltage. Accordingly, designing highly accurate fabrication devices for addressing the major group of permanent faults resulting from imprecise manufacturing is paramount to successful deployment of future reliable systems with deeply-scaled devices operating at low voltages.

### Degradation Effects

Even though if we assume that the circuit has been fabricated precisely and package shielding protects it against both SET and soft errors, the active circuit may still fail due to reliability issues associated with the activity factor of the circuit. For example, the interconnects of the circuit can experience gradual movement of ion in the metal because of momentum transfer from electrons [9]. This phenomenon is referred as electromigration which eventually cause the failure of the affected circuit. Although the continuing miniaturization of the electronic devices has significantly reduced the gate capacitance and supply voltage which in turn cause the current reduction, but the demand for performing the required function with higher frequency has constrained the current density. On the other hand, the metal line width is proportionally reduced with shrinking the technology node which result in increasing current density in the wire cross-sectional area [9].



Beside the electromigration concern in the interconnections, the transistors are also subject to another reliability issues associated with aging-related degradations. *Negative Bias Temperature Instability (NBTI)* and *Hot Carrier Injection (HCI)* are two major aging degradation threats that can manifest themselves as delay increase which might result in timing errors in the critical or near critical paths of the circuit [10]. In addition, the High-K/Metal Gate utilization in the structure of transistor has given rise to *Positive Bias Temperature Instability (PBTI)* along with NBTI [11]. Generally, the above transistor aging effects cause a cumulative degradation in the threshold voltage  $V_{th}$ , of both nMOS and pMOS transistors which leads to slower circuit operation over its lifetime. If such delay degradation is not budgeted or compensated for, then the circuit eventually fails to perform correctly within timing constraints. A common methodology in the consumer electronics market is to under-clock the circuit as compared to what it was designed to operate under ideal conditions. However, this worst-case approach may not be feasible for all application domains and in most cases, the maximum possible performance is sought.

Figure 2 shows the lifetime of the circuit implemented by different technology nodes. The normal execution period has gradually reduced by moving towards downscaled technology node due to increasing probability of failures such as oxide wearout, electromigration, and aging effects in the deeply-scaled circuits.

### The BTI Phenomenon

Generally speaking, the NBTI is considered the primary source of reliability issue in the submicron manufacturing era before the technology advancements enable us to fabricate the

transistors with sub 28nm technology node. Yet, the utilization of High-K material in the sub 28nm transistor's structure for maintaining the drain current while improving the oxide capacitance has changed the ratio of PBTI contribution to the BTI issue. The performance degradation due to PBTI is gradually increasing as the technology rapidly scales down. We briefly describe what circumstances result in the NBTI and PBTI phenomena in the next section.

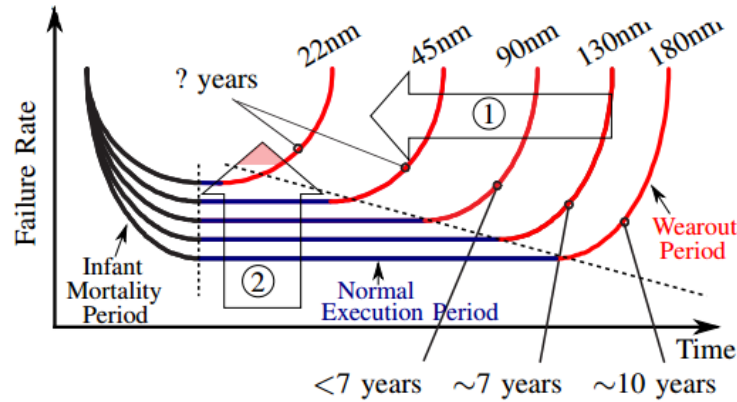


Figure 2: Increasing failure ratio due to accelerated transistor aging (1) and vulnerability to soft errors (2) [12] [13].

### The NBTI Process and its Impact on the Circuit's Lifetime

Two generally accepted assumptions for  $V_{th}$  shift in the aged circuit, which are also coincide with the scientific observations are as following: 1) the generation of hole trapping in the dielectric bulk [14], 2) the break  $Si-H$  bonds at the gate dielectric interface due to the interaction between holes in the inversion layer and hydrogen-passivated  $Si$  atom [14] [15]. The second assumption can also create positively charged interfacial traps and release neutral  $H$  atoms [15]. The generated hole trapping in the dielectric bulk, the broken  $Si-H$  bonds and the positively charged interface traps at the gate dielectric interface due to NBTI stress have been shown in the Figure 3. It has been reported in [15], [16], [17], [18], [19], [20] that the NBTI

effect on the lifetime operation of the circuit is a function of runtime parameters such as temperature, signal probability, duty cycle, and voltage profile.

It is worthwhile to mention that even the NBTI stress results in the performance degradation in the system, the device under NBTI stress is entered to the recovery phase while it is turned off [14]. The recovery phase of NBTI has been investigated by various researcher [21], [22], [23]. The authors of [23] reported that the stressed device can partially recovered after stress removal. On the other hand, [22] showed that the stressed device exhibits complete recovery by switching the device off. The recovery phase starts by returning the freed  $H$  atoms towards the dielectric interface and alleviating the broken  $Si-H$  bonds as shown in Figure 3, thus the absolute value of the  $V_{th}$  is reduced [14].

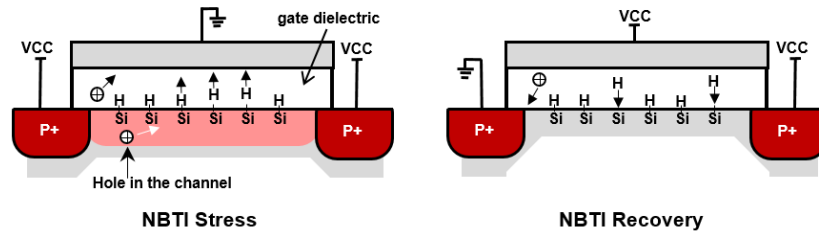


Figure 3: The NBTI stress and recovery illustration (based on [14] and [24]) .

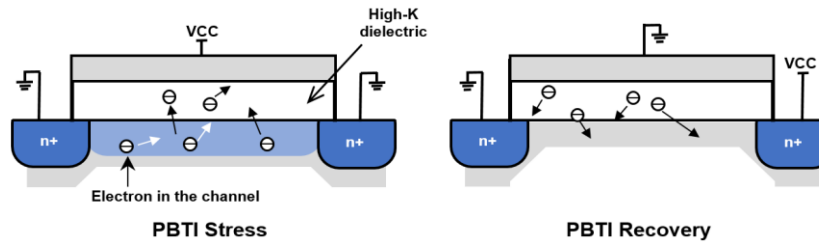


Figure 4: The PBTI stress and recovery illustration (based on [14] and [24]) .

## The PBTI Process and its Impact on the Circuit's Lifetime

Even though the NBTI has been recognized as the major source of the transistor degradation, the gradual rising performance degradation due to PBTI has undermined the benefits of introducing High-K/Metal Gate for improving the oxide capacitance. The operation of this relatively new material under either stress phase or recovery phase is not still entirely clear to the researchers. However, it is generally accepted that the threshold voltage of nMOS is shifted under stress condition because of electron trapping at the gate dielectric interface as illustrated in Figure 4 [24] [25]. Nonetheless, the  $V_{th}$  degradation is partially or completely alleviated by diffusing back the trapped electrons towards the dielectric interface in the recovery phase [25].

## The BTI Physics and Aging Model

For BTI, the contribution of interface traps and traps inside the dielectric layer are addressed. Both a Charge *Trapping/Detrapping* (TD) model and a *Reaction-Diffusion* (RD) model have been utilized in the literature to account for these effects [26]. For instance, compact modeling of aging under DVS for both TD and RD mechanisms is presented in [27].

The Eq. 1 expresses the stress-time induced contribution of Interface Traps (IT) to the  $V_{th}$  shift [28]:

$$\Delta V_{th,IT}(t) \sim \exp\left(-\frac{E_a}{KT}\right) \left[\frac{\varepsilon}{t_{ox}}(V_{gs} - V_{th})\right]^A \exp[B.E(V_{gs}, V_{ds})] t^C \quad (1)$$

along with Oxide Traps (OT) inside the dielectric [Tudor et al. 2011]:

$$\Delta V_{th,OT}(t) \sim \exp\left(-\frac{D + \frac{F}{T}}{E(V_{gs}, V_{ds})}\right) t^G \quad (2)$$

where:

- A denotes the inversion charge exponent,
- B denotes the oxide electric field dependence,
- C denotes the stress time exponent for IT,
- $E(V_{gs}, V_{ds})$  denotes the electric field strength,
- F denotes the temperature dependent component, and
- G denotes the stress time exponent for OT.

Thus, Eqs. 1 and 2 govern aging behavior during intervals of stress. Meanwhile, the partial recovery effect is modeled by taking into account the stress-stimulus duty cycle. When recovery is taken into account, the net impact on the  $V_{th}$  shift becomes [28]:

$$\Delta V_{th,AC}(t) = \Delta V_{th}(t) \cdot \exp(-J.K) \quad (3)$$

where:

- H denotes the transient degradation parameter,
- J denotes the duty cycle dependent exponent for transient degradation, and
- K models the effect of the duty cycle.

These relationships are utilized by the commercially-available MOS Reliability Analysis (MOSRA) tool for Synopsys HSPICE.

The delay at the gate-level under BTI due to  $\Delta V_{th}$  can be expressed as:

$$D_i(t) = \frac{C_i V_{DD}}{\beta_i [V_{DD} - (V_{th} + \Delta V_{th}(t))]^\alpha} \quad (4)$$

where,  $\beta_i$  is a constant which is dependent on the area of the gate,  $C_i$  is the effective load capacitance of the gate and  $\alpha$  is the saturation velocity index. Clearly, an increase in transistor's  $\Delta V_{th}$  from the initial value  $V_{th}$  results in an increase in the delay at logic gate-level.

### Categories of BTI Mitigation Methods

Over the years, many techniques for compensating transistor aging have been presented in the literature. They range from static design-time approaches to dynamic runtime management approaches. Most approaches will result in some area, power, or performance overheads, while others try to leverage idle-time of the applications to mitigate aging through power-gating. Most design-time approaches depend on the use of predictive aging models to *proactively* decelerate the aging process within the circuit. However, such design-time modeling can be complicated as it requires an estimate of runtime operating conditions including input workload.

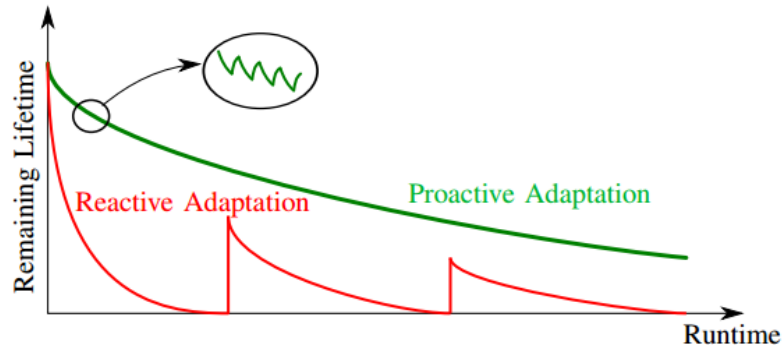


Figure 5: Proactive vs. reactive techniques [12].

On the other hand, the dynamic runtime anti-aging schemes are introduced to avoid the incurred overheads of pro-active scheme. These *reactive adaptation techniques* require some sort of on-chip feedback management system to assess transistor-aging during operation. Figure 5 shows the circuit lifetime implemented by proactive and reactive adaptation techniques whereby the reactive techniques remain deactivated until the aging rate passes a threshold while the proactive adaptation technique maintain the aging ratio as low as possible prior to reach the aging threshold.

### Contribution of Thesis

Based on the vast investigation on the previous BTI prediction and mitigation techniques, a comprehensive survey for some related techniques will be presented in the following chapters. Our focus will be to classify the existing research works based on their contributions into three categories: 1) *BTI aging prediction*, 2) *BTI aging measurement*, and 3) *BTI aging mitigation*. First, the previous BTI prediction techniques are reviewed which are utilized to estimate the amount of performance degradation over the operational period of a device. Next, we discuss existing aging-detection sensors which are used to enable the real-time aging-compensation mechanisms through actively monitoring the transistor parameters or performance degradation. A concise survey of BTI aging mitigation techniques will be presented after the aforementioned sections to provide a conceptual overview to the reader.

Furthermore, we will investigate the effect of BTI on the elements utilized in the power-gating technique which is one of the well-known BTI mitigation methods. Power-gating reduces the duration of the circuit operation and hence power consumption as well as temperature, both

of which can decrease BTI effects. Furthermore, the stress interval of MOS transistors is reduced because a power-gated MOS transistor enters a recovery condition due to clearing of interfacial traps. In order to utilize power-gating techniques, a transistor inserted into the header and/or footer called a *Sleep Transistor (ST)* is inserted to realize a pull-up and/or pull-down supply network to provide a virtual  $V_{DD}$  or  $V_{SS}$ . The ST reduces the leakage current that flows in the supply-ground path when the circuit is in its stand-by mode which is known as sleep mode. However, the ST suffers continuous BTI stress during active mode and can age significantly. The aging impact will aggravate the performance degradation of the logic circuit in a power-gating structure. NMOS devices exhibit a smaller threshold voltage shift than PMOS devices under the effect of NBTI [29]. Conversely, PBTI on NMOS can be the dominant degradation mechanism. Accordingly, the power-gating model used in order to mitigate a BTI effect is important. The comparison results among different ST implementation are elaborated in chapter five.

To address all these concerns, we will introduce an *adaptive resource management* anti-aging approach at the circuit level with low overhead. Essentially, each critical logic path is determined and remodeled at design-time based on the allowable area overhead, performance requirements and the expected level of reliability. During the circuit's operation, only one instance in the pool of identical logic paths is selected for executing the required function. Each instance selected from the pool of identical logic paths across the entire circuit is equipped by a sensor which continuously monitors the aging pace in that particular instance. If a timing violation occurs in a particular instance, the aged logic instance is power gated while another identical instance from the pool is selected for continuing the operation of the aged instance. A detailed elaboration of the proposed technique will be provided in Chapter 6.



## Organization of Thesis

This thesis is organized into seven chapters. Figure 6 outlines the materials that each chapter covers. We elaborate some aging prediction techniques in which the lifetime reliability of the circuit is characterized in Chapter 2. The aging measurement techniques utilizing either in-situ sensors or replica circuits for circuit degradation assessment are introduced in Chapter 3. Chapter 4 discusses the related works for mitigating the effect of BTI. The impact of BTI on the elements used in power-gating technique is introduced in Chapter 5. The power consumption and delay degradation associated with employment of different power-gating techniques are also provided in this chapter. Chapter 6 introduces the technical detail of the proposed adaptive resource management anti-aging approach. Chapter 7 concludes the thesis.

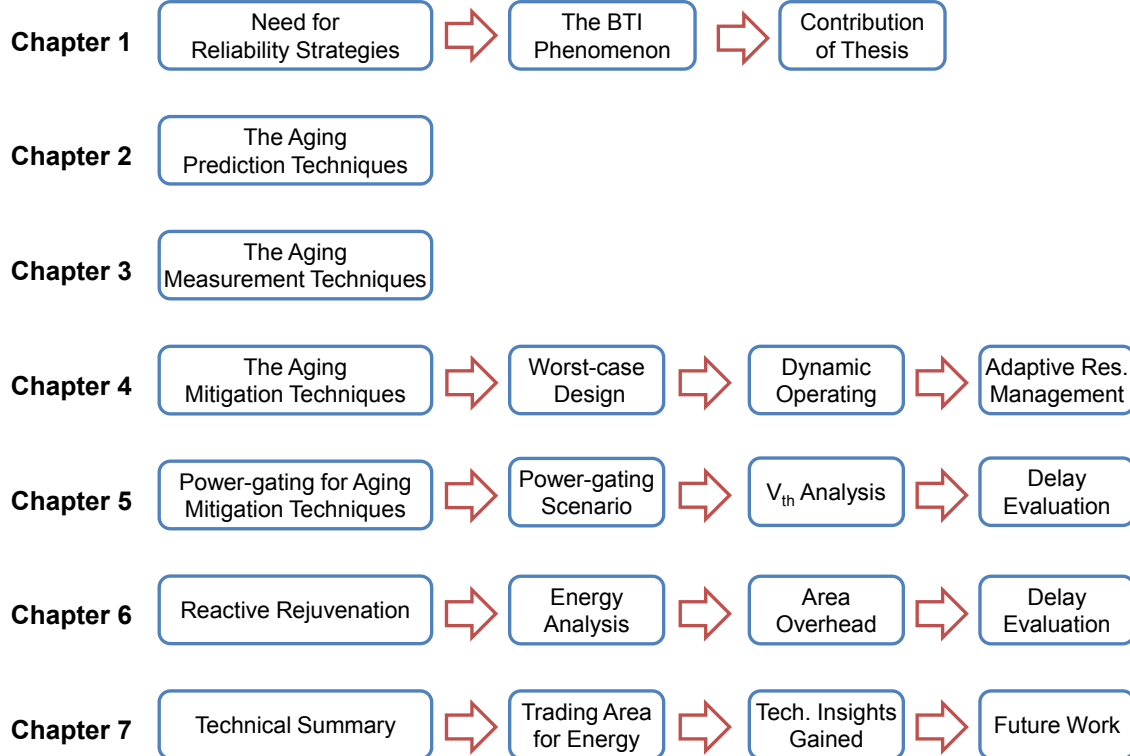


Figure 6: Organization of Thesis

## CHAPTER TWO: THE AGING PREDICTION TECHNIQUES

The main objective of the aging prediction techniques is to characterize the lifetime reliability of the circuit at design-time. Some research works have also integrated their aging model into the *Statistical Timing Analysis (STA)* framework to optimize the design timing using conventional design EDA tools. Accommodation of factors such as process variation, signal probabilities, etc. into STA help in automation of the process of design-time guardbanding using area, voltage, or frequency margining [30], [16]. Generally, this worst-case accommodation results in high overheads.

Aging-aware logic synthesis is also conducted by using multiple timing constraints based on estimated aging rates. A comparison between various aging prediction techniques has been shown in Table 1. The comparison between various approaches is done based on the number and nature of parameters considered during the modeling of aging degradation over time, and whether the technique is feasible for integration into conventional EDA toolchain, which is key for easy adoption of the techniques. The large number of parameters required for the models, requires the use of complex optimization techniques.

In [30], the effects of both fabrication-induced process variation and runtime aging are considered in the statistical gate delay aging model. While the integrated circuit is fabricated, the variation in the transistors' specifications results in producing the circuit paths made by non-uniform transistors having variable initial threshold voltage and oxide thickness. The random nature of process variation results in the impact of NBTI on the lifetime performance of the circuit also becomes a random process. In order to represent the random impact of NBTI aging

process, the stochastic collocation method [31] is integrated into the proposed gate delay model while the parameters of process are considered as random variables with normal distribution. This consideration enables the proposed STA framework to accurately estimate the lifetime reliability of the circuit by extracting the correlation among the selected path under stress and process parametric variations.

The authors of [16] enhanced the aging model at the gate level by taking the workload information at the gate inputs into account along with other influential aging parameters such as operational lifetime, temperature, and supply voltage. The workload information is dependent on the signal probability and transition density. This information is given to the gate delay model to precisely profile the gate performance degradation while the transistor is under stress condition. In order to make the proposed model applicable for aging estimation in the multi-stage gates such as *AND* and *OR*, the signal probability and transition density for the internal nets of the gate needs to be considered. Accordingly, this method splits each multi-stage gate into several single-stage gates and utilizes a probabilistic method to calculate the aforementioned parameters for the internal nets of the decomposed gate. Furthermore, they have extended their approach from gate granularity to Macro Cell granularity to speed-up the timing analysis of the entire circuit by reducing the timing graph which represents the timing model of the circuit. Basically, the pool of elements in the proposed timing graph is constrained to those elements which belong to the critical or near critical logic path.

The authors of [17] proposed an aging-aware timing optimization technique to target only a sub-set of critical and near critical sensitizable paths for optimization. To identify whether a path is sensitizable or not, the *timed automatic test pattern generation* (timed ATPG) [32] is

employed to feed the circuit with the combination of the potential input patterns. If at least one input set activates the path, this path is considered as sensitizable path. Next, the SAT solver is modified to extract the sub-circuit that covers all possible sensitizable paths. To minimize the circuit delay due to BTI reliability issue, the proposed algorithm iteratively applies the logic reconstruction and pin reordering [33] on the critical sub-circuit while the transistor resizing and path sensitization are considered. As a result, a significant portion of gates are excluded from the optimization process which makes this approach runtime efficient and highly scalable while incurring low area overhead.

The proposed idea in [18] is inspired by the fact that currently used synthesis approaches balance the circuit timing at design-time without considering the impending delay due to aging issue for each path. In this regard, the paths with larger timing slack are slowed down for balancing the delays which relatively saves the area. However, the area reduction of these paths come at the expense of increased aging ratio whereby the non-critical paths might become critical over the circuit's operational lifetime. To improve the overall lifetime of the circuit, the aging-sensitive paths are redesigned to be executed faster which incurs more area overhead to the system. To compensate this overhead, the paths with shorter timing slack are redesigned to be executed slower while their timing constraints are correspondingly relaxed. Thus, the consideration of the post-aging delay while optimizing the circuit timing significantly improves the overall lifetime of the aging-susceptible circuit which results in all paths reach the desired guardband at the same time.

An additional design-time technique of aging-aware logic synthesis is proposed in [34] where multiple timing constraints are applied on different logic paths based on the available

timing slacks and aging rates. The key innovation of this work is to synthesize microprocessor pipeline stages which are balanced in terms of Mean-Time-to-Failure (MTTF) instead of the traditional approach of delay-balanced pipelines. Here, tighter timing constraints are obtained through a combination of gate-sizing, logic path re-organization or time borrowing or by using low- $V_{th}$  gates.

The beauty of the proposed technique in [19] is that the runtime variation at the system-level granularity is extracted to enhance the accuracy of delay estimation in the circuit-level granularity. To achieve this goal, the target application is executed on a full computer simulator to capture the workload profile including input pattern and power information. Next, the logic simulator is fed by workload profile and gate-level netlist to extract the signal probability and switching activity of each transistor. Then, the voltage and temperature at gate-level granularity are obtained based on the provided information from the previous step to accurately estimate each gate delay due to induced BTI. As a result, the circuit delay can be accurately estimated by considering the gate delay as a function of  $V_{th}$  shift, temperature and voltage in the STA tool. The integration of this framework into commercial EDA tool chain can provide the scalability for large-scale circuit designs. In addition, the proposed automated aging analysis methodology demonstrated in [20] enables the circuit designers to benefit from the fast and highly accurate aging prediction methodology which has also been integrated into the commercial STA tool (Synopsys PrimeTime).

The iterative optimization process through the use of commercial synthesis tools is attractive, although the authors report in [18] that it may not converge and the area overhead may be excessive in some cases. Furthermore, such High-Level Synthesis (HLS) techniques [35]

assume the availability of a standard cell library characterized with aging delays which can guide the synthesis process to utilize optimal-sized/ $-V_{th}$  logic gates such that desired lifetime is achieved.

Table 1: Comparison of aging prediction techniques.

<b>Aging Prediction Technique</b>	<b>Considered Parameter in the Model</b>	<b>Integration into Commercial Tool Identified</b>
Lu et al., 2009 [13, 30]	temperature, signal probability, duty cycle, process variation, voltage variation	no
Lorenz et al., 2010 [16]	temperature, signal probability, circuit lifetime, workload profile	no
Wu et al., 2011 [17]	temperature, signal probability, circuit lifetime	no
Ebrahimi et al., 2013 [18]	temperature, signal probability, switching activity, circuit lifetime	yes
Firouzi, Kiamehr, Tahoori, et al., 2013 [19]	temperature, signal probability, switching activity, power-voltage profile, workload profile	yes
Karapetyan et al., 2015 [20]	temperature, signal probability, transistor density, circuit lifetime, voltage profile	yes

## CHAPTER THREE: THE AGING MEASUREMENT TECHNIQUES

Some anti-aging techniques downplay the use of aging prediction through the use of on-chip sensors for in-field measurement of transistor aging. Many aging sensors have been proposed in the past to accurately monitor the transistor parameters or performance degradation of the active devices. The proposed aging sensors can be categorized from those based on Metal–Oxide–Semi-Conductor Field-Effect Transistor (MOSFET) parameter sensing [36], to those that are rely on propagation delay measurement through ring oscillator [37], [38], [39]. The output of these aging measurement techniques can be used as a control signal in the aging-mitigation methods to overcome the performance degradation due to aging phenomena. In addition, the on-chip aging sensor is required to exhibit low sensitivity to PVT (process, power supply voltage and temperature) and impose reasonable area overhead to the circuit design [39].

Initially, in order to measure the BTI effect, the BTI-induced parameters were directly sensed. Although this early stage technique was efficient in the beginning, the researchers understood over time that the direct MOSFET parameter sensing can introduce the large recovery while characterizing the BTI effect. Thus, the BTI measurement techniques which introduce zero recovery while determining the actual degradation under BTI stress became favorable. The proposed BTI sensor in [36] works through monitoring the small voltage drift via on-the-fly measurement without having recovery effect on the sensed transistor. However, this technique requires off-chip measurement circuits such as voltage reference which makes it potentially unfavorable for utilizing in the circuits with limited power budget.

On the other hand, instead of measuring the BTI directly, the propagation delay can be considered as an expression of the BTI effect. In [40], an on-chip sensor which monitors the frequency degradation of the circuit is presented. The two *Ring Oscillators (RO)* are devised to be employed in the structure of this sensor device. The reference RO is considered as the reference to determine the amount of frequency degradation in the stressed RO. Accordingly, the reference RO is kept unstressed while the other RO is periodically stressed. In particular timestamp, the phase comparator is activated to measure the frequency difference between these two ROs. This comparator produces a beat signal which represents the frequency proportional to the aging effect. Next, the generated beat signal is fed to a counter to quantify the amount of degradation. The utilization of two ROs in this design improves the sensing resolution by 50X compared to the limitation of the previous techniques which proposed to only use a single RO in their structure.

In order to translate the frequency degradation to  $V_{th}$  shift, the calibration methodology proposed in [31] can be utilized. However, since the BTI-induced degradation cannot be quantified based on the amount of  $V_{th}$  shift due to NBTI and PBTI, it might not be an appropriate technique to be employed as sensor for a particular BTI reliability issue. Nonetheless, the same pair RO architecture is modified by the authors of [37] to separately quantify the aging effects of HCI and BTI.

The authors of [38] proposed a compact NBTI sensor which works based on the fact that, by increasing the  $V_{th}$  due to NBTI, the frequency of RO significantly reduces. This sensor enables the chip testers to digitalize the NBTI stress in the subthreshold region. However, the



operation of this design in the subthreshold region suffers from nontrivial sensitivity to temperature variation.

Recently, the HCI has manifested itself as a critical reliability issue due to manufacturing transistors with the gate lengths shorter than 50nm [39]. The NBTI/HCI on-chip aging sensor proposed in [39] measures the threshold voltage difference between a stressed device and fresh device through the deployment of a threshold voltage detector and a comparator. The proposed sensor circuit offers a resolution of 1 ns per 0.01 V threshold voltage shift.

The authors of [41] proposed an on-chip aging sensor which is able to isolate the NBTI and PBTI aging effect. For determining the impact of NBTI, two identical NBTI sensors are embedded in this design. Again, the delay difference comparison idea between the stressed sensor and the reference sensor is utilized. Both sensors are fed by a specific duty cycle which results in the reference sensor remaining isolated from this trigger signal while the other one is aged. As a results, the longer propagation delay is observed in the aged sensor. In order to measure the PBTI effect, the same structure is utilized with the difference being that the pMOS devices are replaced by nMOS devices.

Although the concept of using RO for monitoring aging incurs small area overhead and zero performance penalty [42], it still cannot adequately represent the operation function of the circuit which experience the complex workload interdependency over time. To provide an accurate aging measurement technique, the authors of [42] came up with the idea of resembling the topology of the critical and near critical paths with *Representative Critical Reliability Paths (RCRPs)* which are able to represent the aging in the critical reliability paths. To reduce the

overhead of these *RCRPs*, the resembled critical paths are synthesized to cover those paths which have the higher degree of shared delay segment.

On the other hand, some techniques have focused on aging-induced performance degradation to detect sequential circuit timing failures [43], [44]. The objective of these works is to use time borrowing concept for compensating the timing delay. However, area overheads and significant power penalties can be incurred using designs with such specialized sequential elements.

Apart from aforementioned aging measurement techniques, there are some commercial tools such as [45] which consists of both hardware and software packages required for quick and accurate BTI test applications, as well as general characterization. Table 2 provides a qualitative analysis of the aging measurement techniques which will be presented in the final manuscript.

Table 2: Comparison of several aging sensors (as adapted from [41]).

<b>Sensors</b>	<b>Sensed Variable</b>	<b>NBTI</b>	<b>PBTI</b>	<b>HCI</b>	<b>Objective</b>
Denais et al., 2004 [36]	$V_{th}$	yes	no	no	characterization
Kim et al. 2008 [40]	frequency	yes	yes	yes	characterization
J. Keane et al., 2010 [37]	frequency	yes	yes	yes	circuit tuning
Karl et al., 2008 [38]	frequency	yes	no	no	characterization
K. K. Kim et al., 2010 [39]	$V_{th}$	yes	no	yes	characterization
Alidash et al., 2012 [41]	delay	yes	yes	no	circuit tuning
Wang et al., 2012 [42]	delay	yes	yes	yes	circuit tuning
Dadgour et al., 2010 [43]	setup time	yes	yes	yes	binary fail detection
Qi et al., 2010 [44]	delay	yes	yes	no	binary fail detection

## CHAPTER FOUR: THE AGING MITIGATION TECHNIQUES

The main objective of BTI aging mitigation techniques is to compensate the aging-induced delay in the active circuit. The conventional approach of adding *guardbands* significantly reduces the performance of the systems while it also conflicts with the primary goal of transistor downscaling for delivering higher performance in shorter execution period. Thus, the focus of the most recent research in this area has been recast to improve the aging-induced performance degradation without adding the costly overheads to the system.

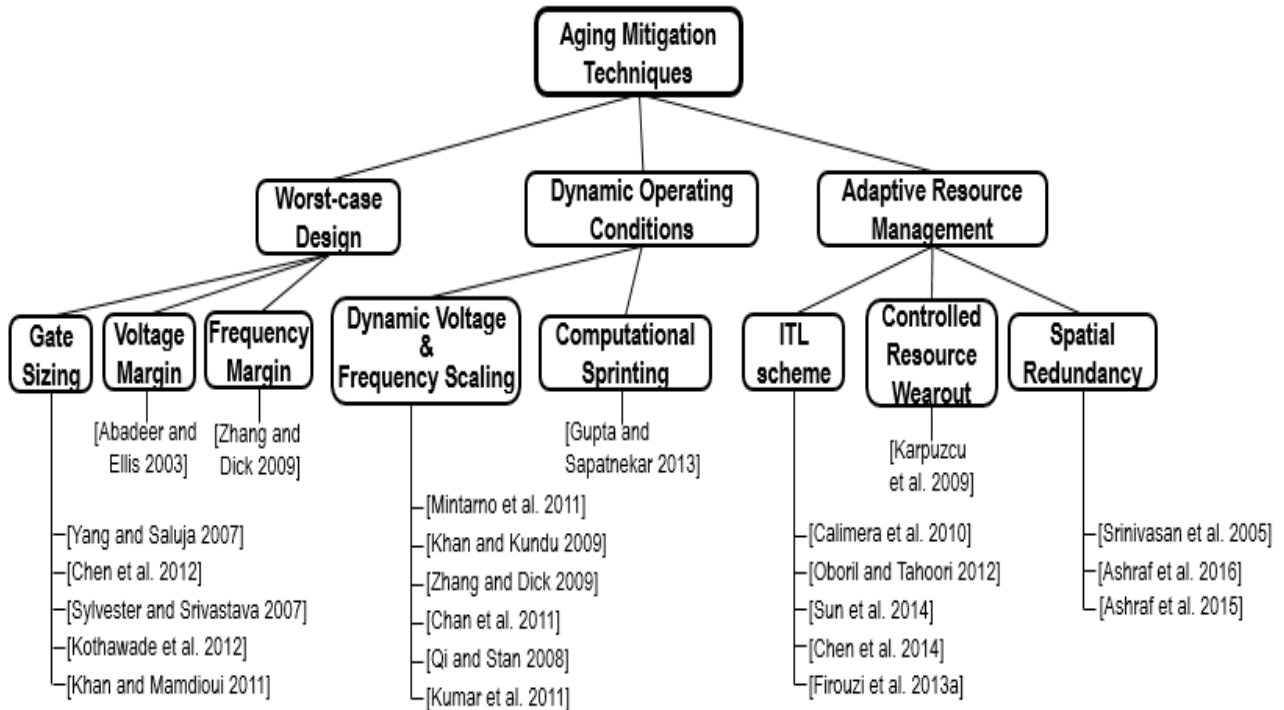


Figure 7: Taxonomy of aging mitigation techniques.

The BTI aging mitigation techniques range from simple one-time static timing margin and voltage guardbanding, up through more complex dynamic adaptation of supply voltage and/or frequency during operation. We have categorized the BTI aging mitigation techniques to three top-level methodologies as shown by the Taxonomy in Figure 7 with details listed in Table 3: 1) *Worst-case Design*, 2) *Dynamic Operating Conditions*, and 3) *Adaptive Resource Management*. These categories are delineated in [46] to provide a means to compare the capabilities and performance of alternative aging mitigation strategies.

### Worst-case Design Techniques for Aging-Compensation

#### Voltage-Margin (VM)

Guardbanding has been used to protect against NBTI which accounts for degradation over the lifetime of a design by reducing the operating frequency or increasing supply voltage, to eliminate BTI-induced timing violations. Unfortunately, provision of a voltage guardband will increase energy consumption over the entire period of operation [15]. Accordingly, guardbanding is known as the worst-case design technique to ensure reliable operation throughout the circuit lifetime. For instance, timing guardbanding (*Frequency-Margin (FM)*) selects the clock period to be more than propagation delay of the aged circuit. Such over-design can also take the form of elevated supply voltage operation (*Voltage-Margin (VM)*) as high as 14.5% over the nominal voltage of an unaged device [47]. This translates to about 30% increase in lifetime energy consumption to compensate for NBTI effects alone. The significance of compensating these overheads is increasing with scaling of technology nodes.

Table 3: Comparison of the aging mitigation techniques [46].

Technique	Anti-Aging Strategy	Design Requirements/ Parameters	Adaptability Characteristics/ Degree	Overheads		
				Throughput	Power	Area
Worst-case Design						
VM, FM	Static Margin	MD-RoD/ $\Delta V_{DD}$ , $\Delta F_{nominal}$	None	FM: High	VM: High (Dynamic & Leakage)	None
Gate-Sizing	Static Margin	MD-RoD; Extended Std. Lib.; Multi-obj. Opt./ $\Delta\beta_i, \forall$ gates $i$	None	None	Medium (Dynamic & Leakage)	Low (Gate-level)
Re-Synthesis	Static Margin	MD-RoD annotated Std. Lib.; Aging-aware Synthesis/ $\Delta\beta_i$ , $\Delta V_{th,i} \forall$ gates $i$	None	None	Low-Medium (Dynamic & Leakage)	Low (Gate-level)
Dynamic Operating Conditions						
DVFS	Dynamic Margin	Timing Sensors; Feedback Control/ $\Delta V_{DD}(t)$ , $\Delta F(t)$ , $\Delta V_{bb}(t)$	Yes/ Fully Autonomous	Low	Medium (Dynamic & Leakage)	Medium (On-chip VR & sensors)
SVS	Dynamic Margin	MD-RoD/ $\Delta V_{DD}(t + \Delta t_{step})$	Yes/ $t_{step}$	None	Medium (Dynamic & Leakage)	Medium (On-chip VR)
GNOMO	Static Margin + Power-Gating	MD-RoD/ ( $V_{DD,g}$ , $t_{idle}$ )	None	Medium (Workload Dependent)	Medium (Dynamic & Leakage)	None
Adaptive Resource Management						
SD	Proactive Mngt. + Power-Gating	Modular Redundancy/ Sleep Interval	Yes/ Sleep Interval	None	High (Leakage)	High (Module-level)
ITL schemes	Proactive Mngt. + Power-Gating	Exploit App. Redundancy/ Idle time	Yes/ Task Scheduling	Medium (Workload Dependent)	None	None
LWL	Proactive Fine-Grain Mngt. + Power-Gating	CPRT/ Sleep Interval	Yes/ Sleep Interval	None	Minimal (Leakage)	Low (Gate-level)
RR	Proactive Fine-Grain Mngt. + Power-Gating	Timing Sensors; Feedback Control; CPRT/ ERT%	Yes/ Fully Autonomous	None	Minimal (Leakage)	Low (Gate-level & sensors)

 MD-RoD: Model-Dependent Rate of  $V_{th}$  Degradation

VR: Voltage-Regulators

## Gate-Sizing

Other worst-case design techniques which utilize additional area to compensate for aging effects include gate-sizing techniques [48] [49]. As indicated by Eq. 4, the delay at gate-level can be decreased by increasing the gate size  $\Delta\beta_i$  from its minimal allowable size  $\beta_i$ . Thus, gate-sizing techniques involve finding optimal sizes for all gates within an allowable discrete or continuous range in the circuit synthesis stage such that all the logical paths meet the desired timing specifications throughout the lifetime. The complexity of discrete gate-sizing is known to be NP-complete, thus mostly heuristics are utilized [50]. Furthermore, this aging-aware synthesis is performed based on assumptions such as knowledge of the stress probabilities at all nodes in the circuit and provision of a standard cell library having logical gates with multiple widths for each stress level. For example, an area overhead of 19.8% is reported for gate-sizing selected portions in a physical register file of a SPARC processor [51]. The area overheads associated with sizing at the gate level can be reduced by adopting more fine-grain sizing and considering the impact of adjacent gates [52], however, it increases the complexity of the sizing problem.

In addition to the area overhead associated with gate-sizing techniques, the increased gate-widths contribute to increasing the effective gate capacitance thereby increasing the dynamic power consumption of the circuit. Furthermore, the gate leakage and subthreshold leakage currents are also dependent linearly on the width of the gates. Hence, gate-sizing schemes directly contributes to both dynamic and leakage powers. Thus, the gate-sizing problem becomes more complicated as these factors also need to be considered during the optimization process. The over-sized gates also undergo continuous stress in the form of elevated temperature

and high signal activities depending on the input conditions while no opportunity for forced recovery is pursued.

### Dynamic Operating Conditions for Aging-Mitigation

A significant drawback of design-time techniques is that they require accurate estimation of aging using anticipatory models such as RD or TD as described earlier, whose accuracy is still under investigation by the research community [53]. The models have only been verified at the individual logic-gate level or on ring oscillator circuits. The authors are not aware of any study which evaluates the accuracy of these aging models on benchmark or real-use-case circuits. Most design-time techniques rely on these models to lower their associated overheads, such as the area overheads of gate-sizing techniques. Thus, in practice over-estimation is used to accommodate the circuit lifetime. Herein, the devised techniques give the explicit provision of control over the delay degradation via the novel control knob of *sleep interval* and hence eliminates the need of accurate aging estimation.

### Dynamic Voltage and/or Frequency Scaling

To overcome the constant overheads associated with voltage guardbanding, the voltage can also be increased gradually from its nominal value at run-time to compensate for delay degradation due to aging (see Eq. 4). In this case, supply voltage can be dynamically adapted,  $V_{DD}(t)$ , to prevent any aging-related failure based on feedback mechanisms whereby aging is monitored using canary circuits or tunable replicas [42], [54]. These canary circuits are assumed to assimilate wearout of the original circuit. On the other hand, timing sensors can also be placed

into the circuit for this purpose [55]. Based on the feedback provided, multiple control policies are devised in [56], [57] to jointly tune parameters such as voltage, operating frequency and dynamic cooling to maximize lifetime energy-efficiency.

Alternatively, if the provision of a feedback mechanism is not available, then *Scheduled Voltage Scaling (SVS)* can be performed whereby the voltage increments and time steps  $\Delta t_{step}$  are determined at design-time [47]. However, DVS is shown to achieve a lifetime (10 years) energy benefit of only 7% with respect to simple guardbanding [58]. Additionally, such schemes assume the availability of a mechanism which can achieve voltage steps on the order of 5-10mV, which require high area-overhead and power inefficient on-chip voltage regulators.

Yet another technique to dynamically mitigate  $V_{th}$  degradation is *Adaptive Body Biasing (ABB)* [59], where the body-biasing voltage  $V_{bb}(t)$  is adapted based on feedback at the transistor level. However, it can be less effective with increased levels of degradation and needs to be combined with other techniques such as SVS and aging-aware synthesis [60].

### Computational Sprinting

An effective aging-mitigation technique *Greater-than-NOMinal Operation (GNOMO)* is proposed in [61] which eliminates the need for complex feedback-based control policies and/or on-chip voltage regulators. As proposed herein, aging recovery is similarly promoted through the use of power-gating. However, to lower the throughput degradation due to power-gating, the circuit is operated at elevated supply voltage,  $V_{DDg} > V_{DD}$ , to increase throughput during bursts followed by idle periods  $t_{idle}$  generated to ensure recovery via power-gating. These circadian rhythms were shown to reduce delay degradation by about 1.3-fold to 1.8-fold.



Even though static or dynamic guardbanding in the form of voltage/frequency margining are effective techniques to combat aging, which do not require any changes at the circuit-level [58]. However, the energy overheads due to static margining are generally high, and the implementation complexities of dynamic margining schemes are also high [53]. To address aforementioned issues, low-complexity and low-overhead anti-aging strategies based on adaptive resource management at the circuit-level will be introduced in the next section.

### Adaptive Resource Management for Aging-Resilience

In this sub-section, a class of anti-aging schemes are highlighted whereby the rate of degradation is balanced over all the resources in the circuit either through management of idle time and task scheduling or availability of expendable resources. Aging-mitigation in these cases include power-gating to enforce recovery, or applying specific input vectors which promote recovery or using differential voltage scaling. Power-gating can reduce degradation of  $V_{th}$  by lowering probability that the transistor is under stress.

#### Idle-Time Leveraging (ITL) Schemes

As mentioned earlier, power-gating has been effectively shown to mitigate transistor aging effects. Schemes such as clustered power-gating [62] have proposed effective ways to reduce the overheads of power-gating, whereby the critical and non-critical portions of the circuit are power-gated using different-sized sleep transistors. However, such works assume the availability or prediction of circuit downtime. For instance, tradeoff analysis between lifetime extension and leakage reduction for a 4x4 Network-on-Chip switch [62] show that with the sleep

probability ranging between 0.4 and 0.9, it is possible to increase the lifetime between 2.5X and 6.67X.

In other applications like modern microprocessor cores, the inherent redundancy in certain structures like the pipelined Execution Stage which has multiple arithmetic units can be exploited [63]. Aging mitigation in this scenario can be achieved by carefully scheduling tasks onto the available resources while simultaneously recovering aging effects through power-gating. However, this comes at a cost of throughput degradation as the power-gated units are unavailable to realize maximum Instruction-Level Parallelism (ILP). Thus, the amount and distribution of idle time is highly dependent on application characteristics and may require changes at the instruction-sequencing level to realize full benefits as reported by authors.

Similar resource scheduling at a much coarse-grain level has been demonstrated for multicore processors [64] or General-Purpose Graphics Processing Units (GPGPUs) [65], whereby tasks are assigned based on stress information at core-level. At runtime, workload assignment is done such that cores are relaxed periodically. The NBTI-aware task mapping for multicore processors is shown to improve MTTF by 30% under considered workloads [64]. Here again, availability of both idle time and idle cores is assumed, which is dependent on the application characteristics or workload.

Some other techniques which assume the availability of idle (standby) time involve applying design-time generated input vectors which promote recovery [66]. In summary, the aforementioned schemes typically require control strategies at hardware/software level to dynamically detect idle times during dynamic operation and perform the required aging-mitigation.

## Controlled Resource Wearout to Improve Performance

The BubbleWrap scheme [67] for many-core systems proposes control strategies with the goal of optimizing either power or performance while managing the amount of aging at the core-level. It utilizes a combination of DVS and task scheduling schemes to overcome the throughput degradation. A set of throughput cores, which are utilized for parallel sections of application and *expendable cores*, which are utilized for sequential sections of application are assumed. These two subset of resources are created based on the rate of degradation of individual cores. The expendable cores, which have shorter life are expended earlier using elevated voltages to obtain higher application performance. Alternatively, the set of throughput cores can be expended for the same power budget, where aging for expendable cores is managed by using voltages below  $V_{DD}$ . The BubbleWrap scheme has similar concerns as found in other DVS schemes and assumes availability of extra resources which can be worn-out.

## Structural Duplication (SD)

The enhancement of logic reliability via indiscriminate *Structural Duplication (SD)*, as demonstrated in [68] can result in prohibitive area overheads. In particular, the approach identified functional elements at a module-level granularity for instantiation as standby components to facilitate an increase in device lifetime. In case of a failure, the standby element can be activated resulting in increased lifetime. Structural duplication is considered feasible only if 100% area cost is acceptable.

### Logic-Wear-Leveling (LWL)

It is possible to utilize fine-grain gate-level redundancy for reducing energy consumption which results in incurring significantly less area overhead. The *Logic-Wear-Leveling (LWL)* technique [69] uses a novel synthesis technique called *Critical Path Replication Tool (CPRT)* to replicate only the timing-critical logic paths rather than the entire circuit as a whole. Next, the *LWL* activates each instances with a round-robin fashion for a certain period while power-gating the unselected critical path instances. By removing the stress condition in the unselected instances, the timing degradation due to BTI is mitigated in the power-gated logic domains. Thus, the wear-leveling effect obtained via proactively alternating between redundant critical paths can save up to 31.98% energy consumption at 10 years compared to the traditional voltage guardbanding.

### Reactive Rejuvenation (RR)

The Reactive Rejuvenation (RR) technique [1] deploys a simple shadow latch based timing sensor [70] to examine the BTI impact throughout the lifetime operation of the circuit. The output data is sampled in two different points in time whereby the earlier sample is stored in the main latch while the latter sample is captured by the shadow latch operating with a delayed clock signal as illustrated in Figure 8. Thus, the aging-induced timing violation can be simply detected by a comparison operation using a simple *XOR* logic gate. By detecting any timing violation in the circuit, an error signal is generated to trigger the feedback device controller for compensating the aging effect. This reactive function block shown in Figure 9, removes the

stress condition in the currently active logic domain by putting it on the sleep mode while another unaged identical critical logic instance remodeled using *CPRT* is activated with a round-robin pattern to continue the function of the aged instance. This design can achieve the delay degradation reduction by a factor of 3.32X compared to uncompensated design.

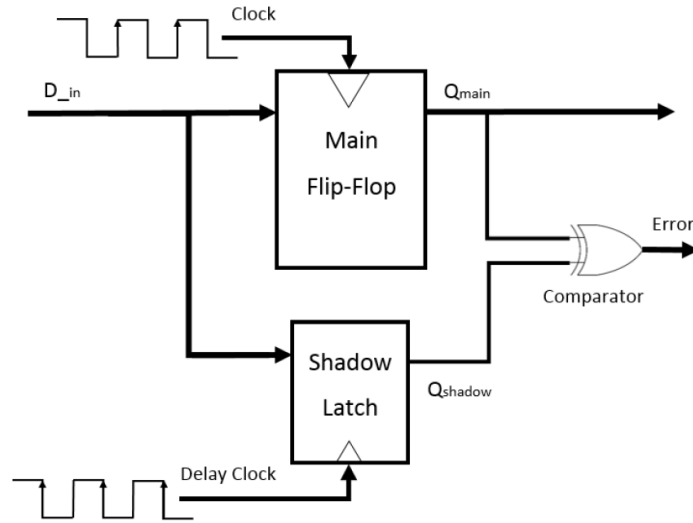


Figure 8: Sampling the output data at two different points in time [1]

### Summary

Transistor-aging is a growing reliability concern in deeply scaled devices, which is often mitigated through design-time approaches, which results in constant high overheads. A comprehensive survey of all techniques presented in the literature is to be done and a taxonomy is to be developed. We seek a technique which can limit the overheads of worst-case modeling through low-overhead dynamic monitoring based on circuit parameter and resource management. The feasibility of integration of the approach in current EDA tools is also essential to foster the full benefits. Addressing these reliability concerns is paramount to successful

deployment of future reliable systems with deeply scaled devices operating at low-voltages.

Based on our background, we presented a comprehensive survey.

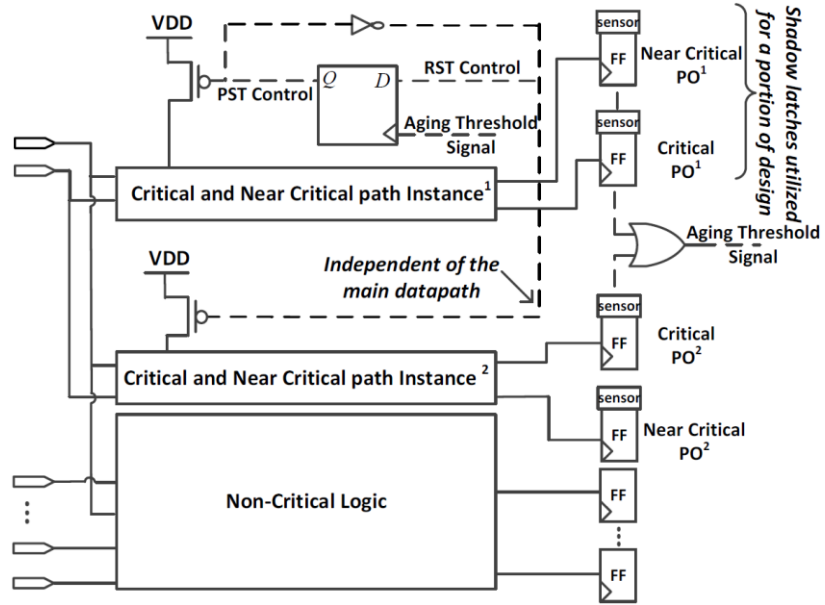


Figure 9: Autonomous aging-aware resource management for  $N=2$  [1, 12]

## CHAPTER FIVE: POWER-GATING STRATEGIES FOR AGING

### MITIGATION OF CMOS LOGIC PATHS

In order to utilize power-gating techniques, a transistor called a *Sleep Transistor (ST)* is inserted into the header and/or footer to realize a pull-up and/or pull-down supply network to provide a virtual  $V_{DD}$  or  $V_{SS}$ . The ST reduces the leakage current that flows in the supply-ground path when the circuit is in its stand-by mode which is known as sleep mode. However, the ST suffers continuous BTI stress during active mode and can age significantly. The aging impact will aggravate the performance degradation of the logic circuit in a power-gating structure [71]. NMOS devices exhibit a smaller threshold voltage shift than PMOS devices under the effect of NBTI [29]. Conversely, PBTI on NMOS can be the dominant degradation mechanism. Accordingly, the power-gating model used in order to mitigate a BTI effect is important.

In order to alleviate aging of ST, several works have been presented previously. The authors of [72] proposed to realize NBTI-aware power-gating through (i) sleep transistor over-sizing, (ii) forward body-biasing, and (iii) stress time reduction. However, the aging of logic networks has not been considered in that work. In [73], authors showed the interdependence between the degradation of logic networks and the ST. In their work, redundant STs are introduced for mitigating the aging of a single ST. This is shown to extend the lifetime of power-gated circuits. With the existence of ST redundancy, the recovery mechanism is explored by recovering redundant STs in a round-robin sequence. Consequently, a sufficient recovery interval is provided to STs for reversing NBTI. Hence, a

decrease in the virtual  $V_{DD}$  due to ST aging is postponed, which mitigates the long-term performance degradation and extends the circuit lifetime. The authors of [74] evaluated the reliability and power consumption benefits of power-gated circuits in 22nm technology under the effects of NBTI/PBTI. They found that power-gating can improve the reliability and provide significant power savings as long as sufficient time for the circuit is provided in sleep mode. For example, [58] reports that to reduce the delay degradation by 5% over an operational period of 10 years, the circuit must remain power-gated for over 60% of the device lifetime which may represent an unacceptable reduction in operational capacity. Thus, alternative approaches have constituted an active area of research [69].

In this chapter, we show the evaluation of the effectiveness of power-gating on PBTI/NBTI phenomenon and propose a preferred ST configuration for achieving improved recovery. In addition, different input frequency signals with the same duty cycle are considered as a case study to obtain more complete results which include the effect of input transitions on the recovery of MOSFET transistors while in sleep mode.

### Power-Gating Scenarios

There are several possible power-gating scenarios based on the location of the ST in the header or footer. To evaluate these, a case study is considered using 50 CMOS inverters which are connected in series, as shown in Figure 10. For the baseline circuit, supply voltage and ground are directly connected without any ST. We implement three different power-gating scenarios in order to investigate the impact of BTI on each of them. In the *Header-based ST (HST)*, we insert a PMOS ST to create virtual  $V_{DD}$  as illustrated in Figure 11. Since the PMOS



ST in power-gated circuit suffers from NBTI in active mode and ages quickly, it degrades the performance of logic elements due to supply voltage changes. One advantage of an HST arrangement is that PMOS transistor exhibits less leakage current than NMOS transistor of equivalent size. The NBTI effect elevates  $V_{th}$  over time and makes PMOS transistor even less leaky. The disadvantage of an HST arrangement is that PMOS has lower drive current than NMOS of a same size. As a result, a HST implementation usually consumes more area than a *Footer-based ST (FST)* implementation.

In FST, we insert a NMOS ST between  $V_{ss}$  and actual ground, shown in Figure 12. The advantage of FST is its high drive current and hence smaller area for equivalent performance. However, NMOS is leakier than PMOS and application designs become more sensitive to ground noise on the virtual ground coupled through the FST. The NMOS ST also suffers from PBTI in active mode which imposes additive performance loss. However, the performance loss of HST and FST circuits is not equal since PMOS ST experiences more dramatic aging effects when it is used in an HST structure in compare to NMOS ST in a FST design. Consequently, HST and FST designs both impact the logic network performance in a different way which are elucidated in this work.

Regarding this observation, we also implement a hybrid power-gating scenario referred to as *Header and Footer ST (HFST)*. HFST corresponds to simultaneous use of PMOS and NMOS STs which help to isolate the transistor gate terminals from electric field stress due to application of inputs during sleep mode. Figure 13 shows HFST design which combines the HST and FST characteristics in this manner.

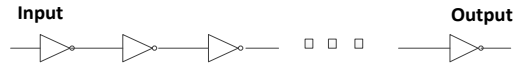


Figure 10: The original circuit

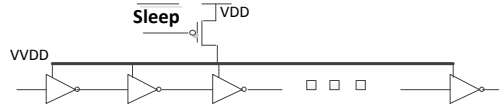


Figure 11: The Header-based ST circuit

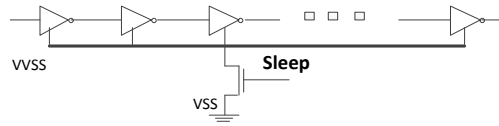


Figure 12: The Footer-based ST circuit

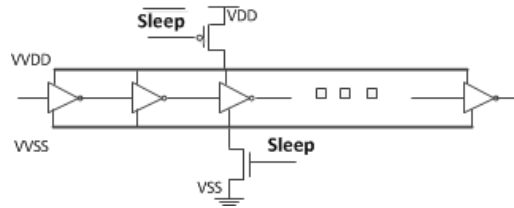


Figure 13: The Header and Footer based ST circuit

A taxonomy of these three alternatives is depicted in Figure 14. It shows the various ST implementation features in comparison for each technique. For instance, HST and FST are influenced more by an NBTI effect or PBTI effect, respectively. Since HFST utilizes both NMOS and PMOS STs in the power-gating implementation, it suffers from both NBTI and PBTI. Furthermore, the PMOS ST channel width in HST approach should be wider to compensate for reduced carrier mobility in comparison to NMOS ST. Consequently, HST

approach imposes approximately two times larger overhead to the ST. Hence, HFST approach endures  $1X+2X=3X$  increase in overhead due to use of both PMOS and NMOS ST in its structure. PMOS ST has a reduced amount of leakage current in comparison to NMOS ST. Thus, HST design exhibits a lower leakage current than FST design. As a result, HFST takes advantage of both HST and FST in its implementation and bears a smaller amount of leakage current.

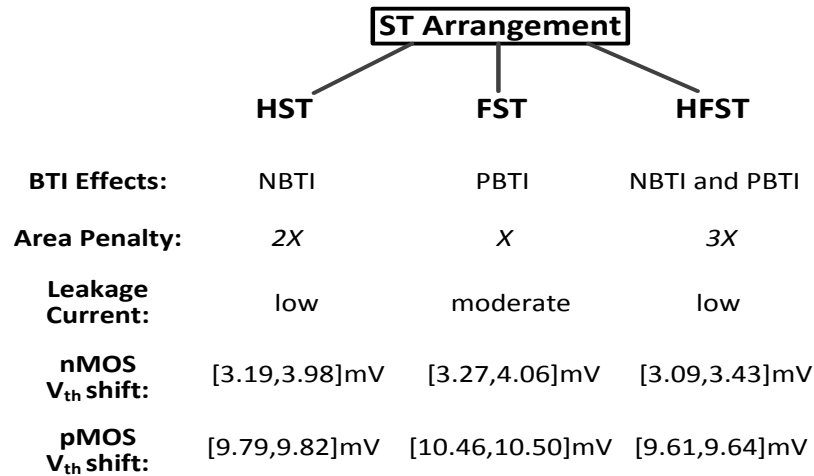


Figure 14: Taxonomy of ST Arrangements and their characteristics

### Experimental Results

To evaluate the above scenarios, the three ST arrangements are subjected to an input squarewave with a 50% duty cycle having a frequency of 1KHz or 100KHz. Each circuit is evaluated under conditions whereby it is in sleep-mode for 70% its lifetime. Consequently, the sleep transistor interrupts the path between the  $V_{DD}$  and ground based on ST arrangement. Our circuit-level modeling is performed via Synopsys HSPICE reliability analysis to simulate BTI effect for the *45nm Nangate open cell library*. In order to apply aging on the inverter chain

circuit, we used MOSRA model [28]. The MOSRA model is constructed with physics-based formulations and augmented with coefficient parameters, to improve the model accuracy and parameter extraction flexibility as identified in the equations below.

### V<sub>th</sub> Shift

NBTI/PBTI effects have two phases of operation depending on the bias condition of a PMOS/NMOS transistor: these are a *stress phase* and a *recovery phase*. In the stress phase, the threshold voltage ( $V_{th}$ ) of PMOS/NMOS increases. During the recovery phase,  $V_{th}$  degradation is partially recovered due to clearing of interfacial traps.

In order to calculate  $V_{th}$  shift, we used the built-in model provided by MOSRA [28]. The MOSRA threshold voltage degradation model provides results which are accurate in numerous aging studies. Two principal physical mechanisms are considered in MOSRA: one is related to the contribution of the interface traps (Equation 5) and the other related to the traps inside the dielectric layer (Equation 6) which are provided here in abbreviated form. In the equations,  $E(V_{GS}, V_{DS})$  denotes the strength of the electric field of the dielectrics. Regarding to the significant dependence of NBTI and PBTI on the channel length, flexible channel width- and length-dependence equations are included in the BTI model of MOSRA.

$$\Delta v_{TH,IT} \approx \exp\left(-\frac{E_a}{K.T}\right) \left[ \frac{\varepsilon}{t_{0x}} (V_{gs} - V_{TH}) \right]^{TITCE} \cdot \exp\left[TITFD.E(V_{gs}, V_{da})\right] t^{NIT} \quad (5)$$

$$\Delta v_{TH,OT} \approx \exp\left[-\frac{TOTFD + \frac{TOTTD}{T}}{E(V_{gs}, V_{ds})}\right] t^{NOT} \quad (6)$$

The partial-recovery effect is modeled by taking into account the stress stimulus duty cycle. When the partial-recovery effect is considered, the total degradation becomes smaller:

$$\Delta v_{TH,AC} = TTD0 \cdot \Delta v_{TH} \cdot \exp(-TD CD \cdot g) \quad (7)$$

where the  $g$  quantity models the effect of duty cycle. As shown in Figure 15 and Figure 16  $V_{th}$  shift in the power-gated circuits is less than the baseline circuit. Moreover,  $V_{th}$  shift in the baseline circuit rises rapidly over time while power-gated circuits have a rather smooth  $V_{th}$  shift. The reason is that the power-gated circuits are in sleep mode 70% of the time which results in much less stress than the baseline circuit. So, during sleep mode, only the recovery phase impacts aging and decreases the aging-induced threshold voltage shift.

### Delay Penalty

Typically, sleep transistors are sized such that a tradeoff among voltage drop, leakage savings, and area overhead is obtained [71]. At the beginning of the device lifetime, addition of a ST will increase the delay. However, the delay penalty decrease as the size of the ST is increased. In this research, the ST has been chosen in a way that the increased delay of the power-gated circuits is less than 3% as compared to the delay of the baseline circuit and the

leakage current is optimum. When we compare the delay of the three circuits, we find that the power-gated circuits have higher delay within 2 years as compared to the baseline, as shown in Figure 17 and Figure 18. However, the power-gated circuits suffer less from aging after 2 years due to the reduced  $V_{th}$  shift.

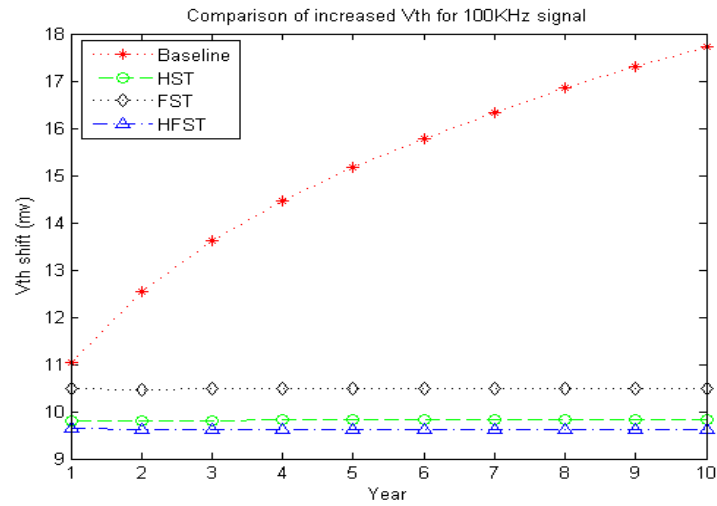


Figure 15: Comparison of increased  $V_{th}$  for 100KHz signal

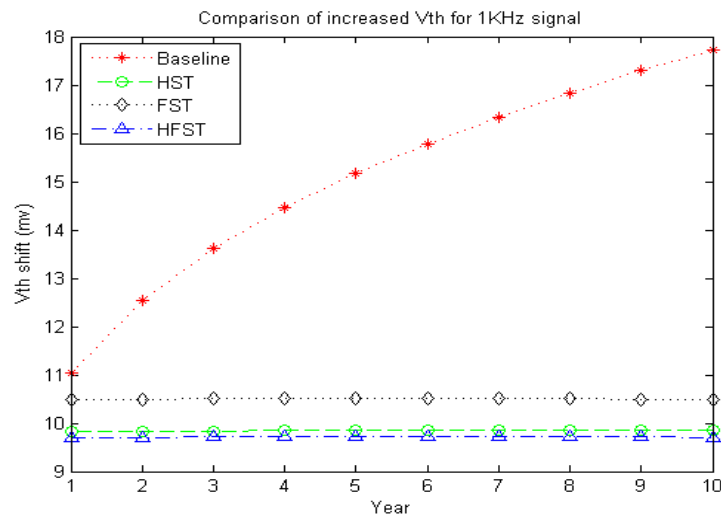


Figure 16: Comparison of increased  $V_{th}$  for 1KHz signal

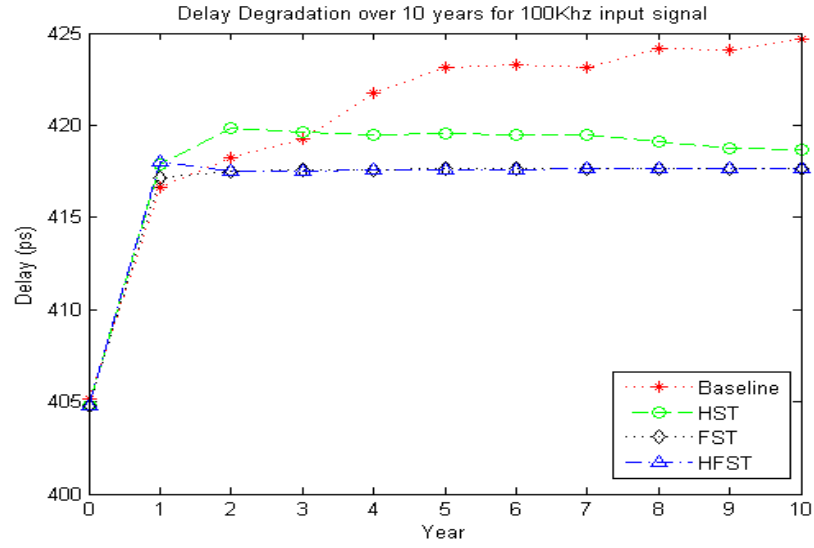


Figure 17: Comparison of increased *delay* for 100KHz signal

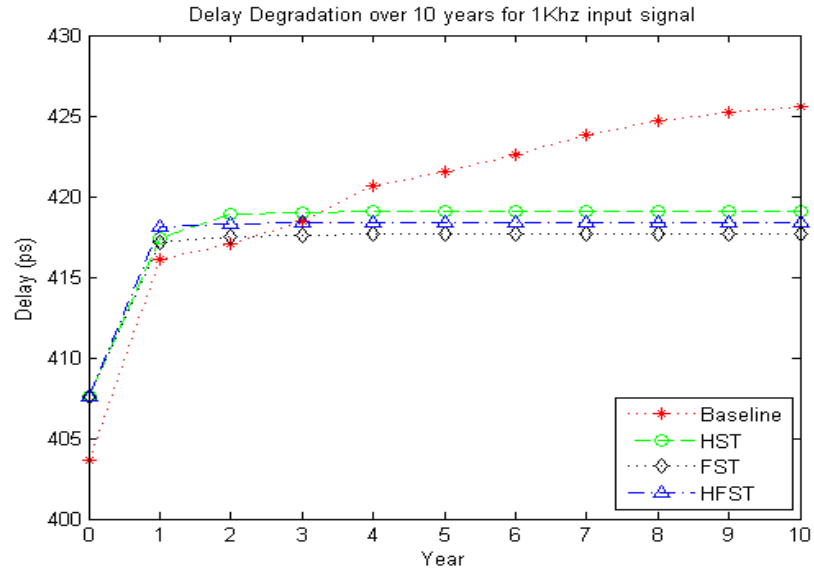


Figure 18: Comparison of increased *delay* for 1KHz signal

### Input Vector Impact on BTI Recovery

It has been assumed that the circuits operate all the time yet practically, not every application requires the underlying hardware to operate at highest performance level all the time. There are periods during which the circuit is not in use, but still affected by the stress induced by the electric field from the application of inputs over a path to ground. This results in the PMOS/NMOS transistors being either under stress or recovery conditions. Although power-gating of portions of the circuit which are not in use may decrease  $V_{th}$  shift, although doing so does not completely recover PMOS/NMOS transistors since they are still under input stress. Figure 19 and Figure 20 demonstrate the comparison of  $V_{th}$  shift for the first three PMOS and NMOS transistors of the Circuit Under Test (CUT) within the inverter chain. The CUT is evaluated in the HST design for 100KHz input signal. The  $V_{th}$  shift for PMOS transistors is around three times greater than  $V_{th}$  shift for NMOS transistors due to further impact of NBTI on PMOS transistors rather than PBTI on NMOS transistors. Moreover, as illustrated in Figure 19, initial transistors in the CUT experience increased aging compared to subsequent transistors, depending on if the circuit is in the sleep mode.

### Analysis and Conclusion

Table 4 shows the comparison of the delay degradation for the circuit which is equipped with different ST arrangements. The delay degradation is between 3.14% and 3.72% for all circuits within the first 2 years of their lifetime which indicates that all arrangements are seen to degrade at similar rates. However, the power-gated circuits suffer less from the aging effect since



they benefit from the less  $V_{th}$  shift after two years. As a result, the delay penalty of the power-gated circuits reduce over time. Table 5 demonstrates power consumption comparison with 100KHz input vector.

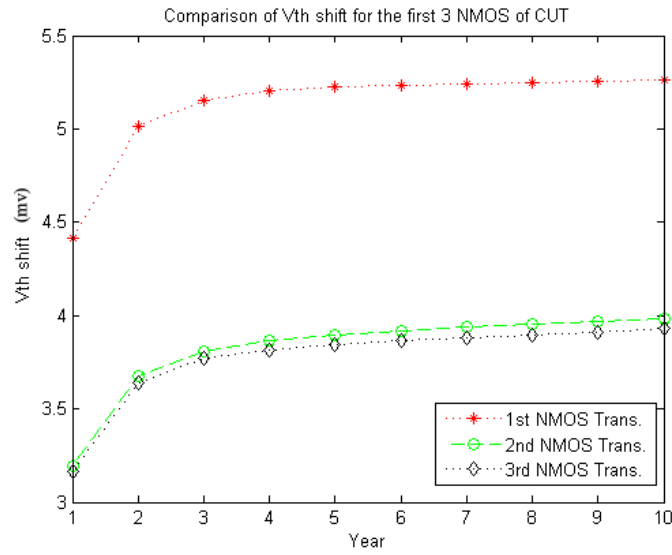


Figure 19: Comparison of  $V_{th}$  shift for the first 3 NMOS of CUT

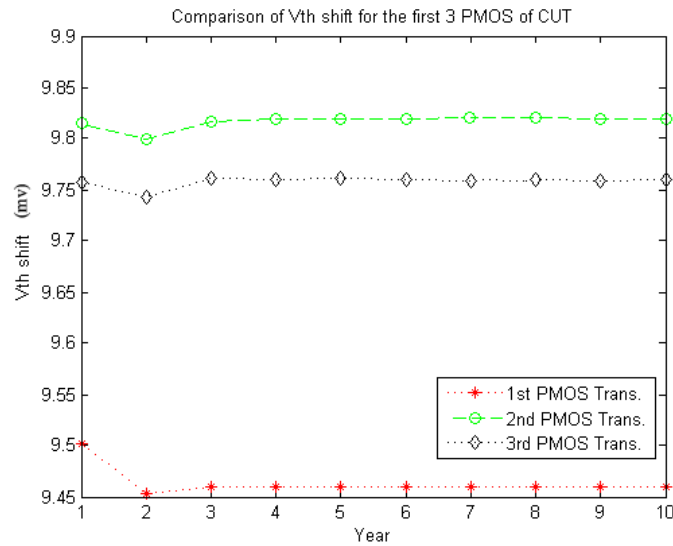


Figure 20: Comparison of  $V_{th}$  shift for the first 3 PMOS of CUT

The baseline circuit is influenced further by the aging effect over time which results in higher  $V_{th}$  shift which reduces the leakage current. Consequently, the trends of power consumption for the baseline circuit shift more than other methods which have relatively constant power consumption.

Table 4: Delay degradation Comparison (% baseline)

<b>Time Method</b>	<b>2 years (%)</b>	<b>4 years (%)</b>	<b>6 years (%)</b>	<b>8 years (%)</b>	<b>10 years (%)</b>
<b>Baseline</b>	3.22	4.10	4.48	4.69	4.81
<b>HST</b>	3.72	3.62	3.64	3.54	3.44
<b>FST</b>	3.14	3.17	3.18	3.18	3.18
<b>HFST</b>	3.14	3.16	3.16	3.17	3.18

Table 5: Power Consumption Comparison (in Watts)

<b>Time Method</b>	<b>2 years</b>	<b>4 years</b>	<b>6 years</b>	<b>8 years</b>	<b>10 years</b>
<b>Baseline</b>	6.64E-07	6.54E-07	6.47E-07	6.43E-07	6.41E-07
<b>HST</b>	6.81E-07	6.79E-07	6.79E-07	6.79E-07	6.78E-07
<b>FST</b>	6.73E-07	6.72E-07	6.72E-07	6.72E-07	6.71E-07
<b>HFST</b>	6.82E-07	6.82E-07	6.82E-07	6.82E-07	6.81E-07

## CHAPTER SIX: REACTIVE REJUVENATION OF CMOS LOGIC PATHS USING SELF-ACTIVATING VOLTAGE DOMAINS

Herein we look toward providing greater improvements in delay degradation, while decreasing the power consumption utilizing spatial multiplexing. Therefore, in this chapter we focus on introducing an adaptive *resource management anti-aging* approach at the circuit level with low overhead. In this work, it is shown that overheads existing in guardbanding approach is significantly reduced. Furthermore, an opportunity is provided for aging-critical portions to recover while avoiding of any significant effects on leakage power. In addition, in the proposed approach the similar advantages of DVS exists without the complexities of dynamic operating conditions at power-network level.

### Bti-Induced Aging Rejuvenation of Aging-critical Logic

If the increased delay due to BTI is not appropriately accommodated, timing failures on critical logic paths may occur. To recover circuit from BTI degradation in the case of timing violation, we develop remodeling of aging-critical logic to meet time constraints and putting the timing critical portions of the circuit on the sleep mode for the purpose of stress relaxation. In some circuits in particular, the distribution of path length allows selective optimizations. It has been shown in [75] that there is a significant spread between the length of the critical path and the majority of paths on an OpenSPARC ALU. Specifically, over 95% of the logic paths exhibit less than 75% of the length of the longest logic path. In practice, various path length distribution seen are an attribute of both the target circuit and synthesis settings used. Here we consider

circuits synthesized with some path length distribution in precedence of the so-called “timing wall” [76].

On the other hand, there may exist some other near critical paths which become critical during circuit lifetime due to varying level of stress. Thus, replicating only a single critical path may not be sufficient. For our experiments, we only select the top 10% of critical paths for replication and protection against cumulative delay variations due to aging effects.

#### Aging-aware Dispatcher for Representative Aging-critical Logic Selection

Over the past few years, several works have attempted to detect timing errors by providing various area/power/detection tradeoffs and granularity of coverage [70] [77]. Shadow latches can be utilized to detect timing violation on the aging-critical logic. These operate by sampling the output data at two different points in time. The earlier, speculative sample is stored in a D Flip-Flop (FF) which is called main FF. This main FF is augmented by a shadow latch operating with a delayed clock signal. Consequently, the timing violation due to BTI can be detected by comparing the two values using an XOR logic-gate as shown in Figure 8. Without loss of generality, an approach similar to the Razor technique [70], one of well-known timing violation detection methods in this area, has been utilized in this work. Figure 21 shows timing diagram in which the main FF and shadow latch capture the same value. Therefore, the error signal remains low.

Figure 22 illustrates timing diagram when BTI increases the delay of the circuit. In cycle 1, the combinational logic exceeds the delay due to BTI. So, both main FF and shadow latch capture input data D in, but in the second clock cycle, transition change of input data D in will be

captured by shadow latch while the main FF still keeps previous D in. By comparing the valid data of the main FF and shadow latch, an error signal is then generated in cycle 2. Without loss of generality, a simple shadow latch based timing sensor is utilized to detect timing error in the BTI-induced aging logic to allow activation of anti-aging voltage domains under localized control.

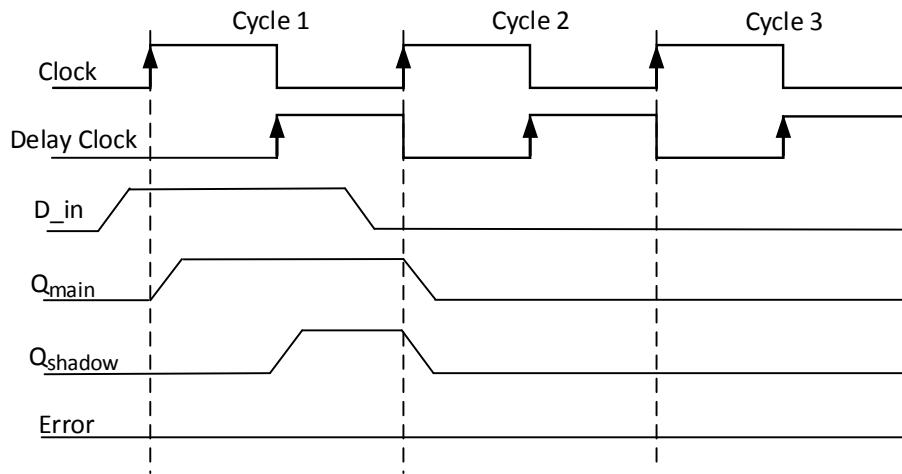


Figure 21: Timing diagram before aging [2, 3]

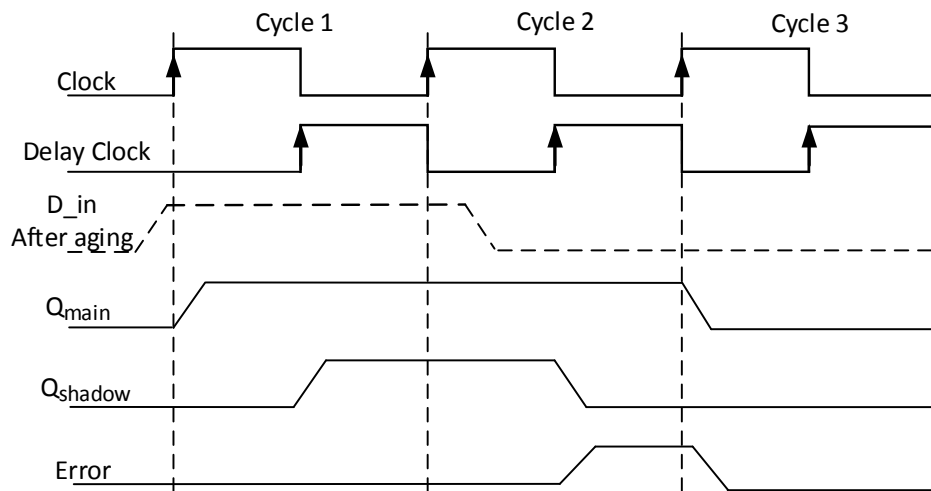


Figure 22: Timing diagram after aging [2]

## Remodeling Aging-critical Logic

The error signal generated by Exclusive-OR gate is used to put the critical path on the sleep mode and active redundant critical path. Thus, circuit can recover from BTI while it is on sleep mode. The proposed idea has been shown in Figure 23. It shows a timing sensitive portion of circuit consists of both critical and near critical paths has been replicated. In order to detect timing violation in the circuit, only the critical path and near critical paths of each instance are equipped by a RAZOR.

When the RAZOR detects any timing violation in the either critical path or near critical paths, it produces an error signal which we call it here switch signal. The switch signal is connected to clock input of a positive edge-triggered D flip-flop. This means that the flip flops can only change output values when the switch signal is at a positive edge. The input signal D is fed by Redundant Sleep Transistor (RST) control signal which comes from the inverted Primary Sleep Transistor (PST) control signal. In the beginning, the RST signal equals to '1' which means the redundant critical path is on Sleep mode. Subsequently, PST signal is '0' which means Critical Path and near Critical Paths<sup>1</sup> functions as usual. When timing violation happens in the primary critical path, this circuit is turned off and disconnected from the  $V_{DD}$  through the sleep. Simultaneously, redundant critical path is turned on.

## Experimental Results

The proposed methodology is evaluated by simulation of `c880`, `i5` and `frg2` circuits from MCNC benchmark suite. Our circuit-level modeling is performed via Synopsys HSPICE

reliability analysis used the built-in model provided by MOSRA [28] to simulate BTI and HCI aging effect for the 45nm Nangate open cell library. The MOSRA model is constructed with physics-based formulations and augmented with coefficient parameters, to improve the model accuracy and parameter extraction flexibility.

HSPICE reliability analysis includes two simulation phases which are stress-free and post-stress simulation phases. In a stress-free simulation phase, HSPICE computes the electron stress of selected transistors in the circuit based on the circuit behavior and HSPICE built-in stress model of BTI effect. According to the information produced during the stress-free simulation phase, HSPICE simulates the degradation effect on the circuit performance in post-stress simulation phase. For the technology node utilized herein, NBTI is seen to be the dominant aging-degradation mechanism.

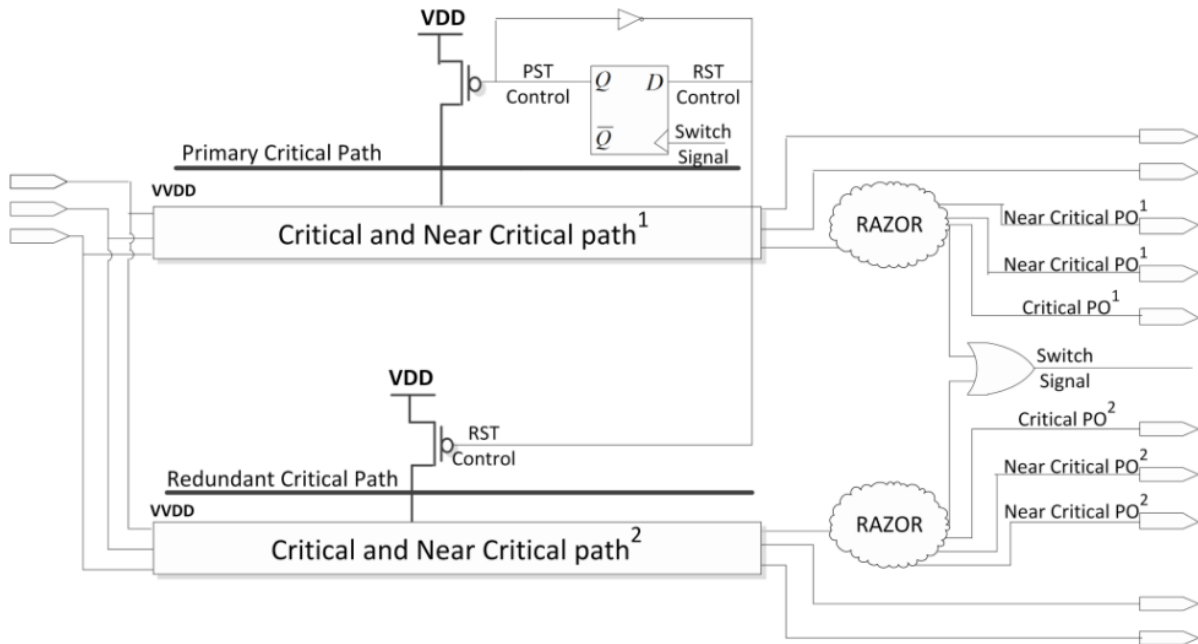


Figure 23: Critical path replication. Here  $CP^i$  denotes  $i^{th}$  instance of the critical path

## Critical Path Remodeling Tool (CPRT)

The EDA design flow used in this work is shown in Figure 24 developed by A. Alzahrani [78]. The RTL Verilog HDL codes for the benchmarks are synthesized and optimized using Synopsys Design Compiler. The worst-case timing paths are determined through applying STA on compiled netlists using Synopsys PrimeTime. The CPRT tool reads and processes the timing report for slowest paths along with the compiled gate-level netlists to re-instantiate cells of selected paths. The CPRT outputs a Verilog HDL netlist of the remodeled design which is functionally verified before a spice netlist is extracted. In order to model the BTI and HCI aging effects, we used the built-in model provided by MOSRA.

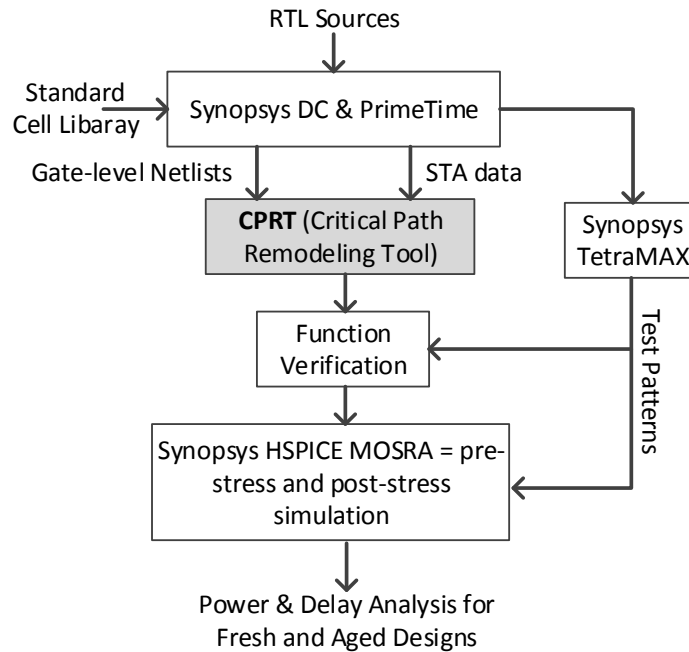


Figure 24: Operation of CPRT within EDA design flow [1].



The Synopsys TetraMAX tool is utilized to generate the minimum number of test pattern required to provide full test coverage for all verification in this work. Even though the flow is automated, the long HSPICE simulation time for large circuits is a limiting factor for circuit size in this study. Thus, results for a limited set of benchmarks is included here.

### RR Reduction of Delay Degradation

In order to evaluate the proposed method, the delay reduction factor is measured over the circuits lifetime. The delay degradation mitigated by RR can decrease the guardbands required for the circuit operation. The experiments for RR are conducted with no timing margin and circuit lifetimes of 3 and 10 years. At design-time, voltage assignment adjusts the circuit's delay to be  $ERT\%$  below the timing specification  $D_{spec}$  by a percentage denoted by the *Elastic Recovery Threshold (ERT)*. Then, RR technique keeps the rate of degradation incurred by the activation of redundant logic domain below  $ERT\%$ . Consequently, RR is able to autonomously adjust its switching interval such that  $D_{spec}$  is never violated.

The minimum switching intervals obtained by RR for  $ERT=1\%$  and  $ERT=2\%$  are listed in Table 6. A reduced switching interval is required to limit the degradation to 1% as compared to 2%. Furthermore, it is dependent on the rate of degradation for a specific benchmark, e.g., i5 has the briefest switching interval due to its highest degradation.

The normalized propagation delay of multiple critical paths over time for c880 using uncompensated design and RR schemes has been shown in Figure 25. The autonomous resource management provided by RR reduces the delay degradation by a factor of 3.32X as compared to

uncompensated design. The advantage of RR comparing to a baseline circuit compensating aging effects by utilizing the voltage guardbands is quantified as total lifetime energy reduction.

The aforementioned effect is shown in Figure 26. Reduced guardbands due to RR enables energy savings as high as 35.3% and 34.6% for `frg2` with ERT of 1% and 2% respectively over 10 years. Highest energy savings are obtained when a lower ERT is utilized. A tradeoff is evident in that a lower ERT% implies more energy savings while a reduced switching interval is required. Low energy operation throughout the lifetime implies that the power constraints of the chip are relaxed.

#### RR Area Overhead

Table 7 shows the initial time Area/Energy overheads with  $N = 2$  at nominal voltage. Here, CGs, AO and EO stand for Critical Gates, Area Overhead and Energy Overhead, respectively. The proportion of the path lengths protected is a percentage of the path length distribution and represented by parameter  $P$ . In this work, our first priority is energy overhead and then we focus on the overhead related to area. The leakage energy of standby Critical Gates (CGs) having significant effect on energy overhead is reduced to a great extent due to power-gating. The area overhead with different values for  $P$  is also provided in the table.

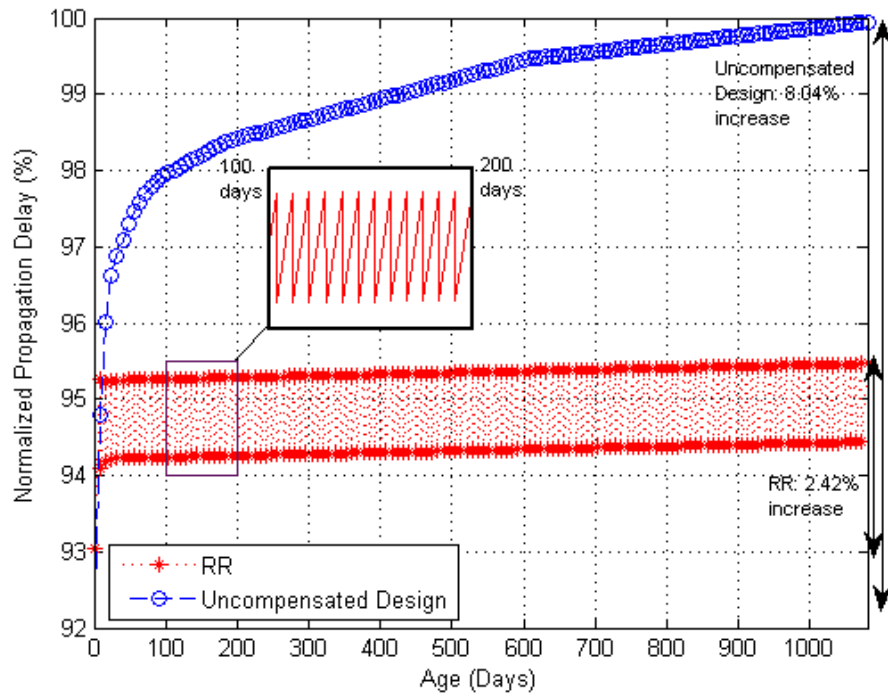


Figure 25: Normalized propagation delay of multiple aging-critical logic over time for c880 with ERT=2% using Uncompensated Design and RR schemes.

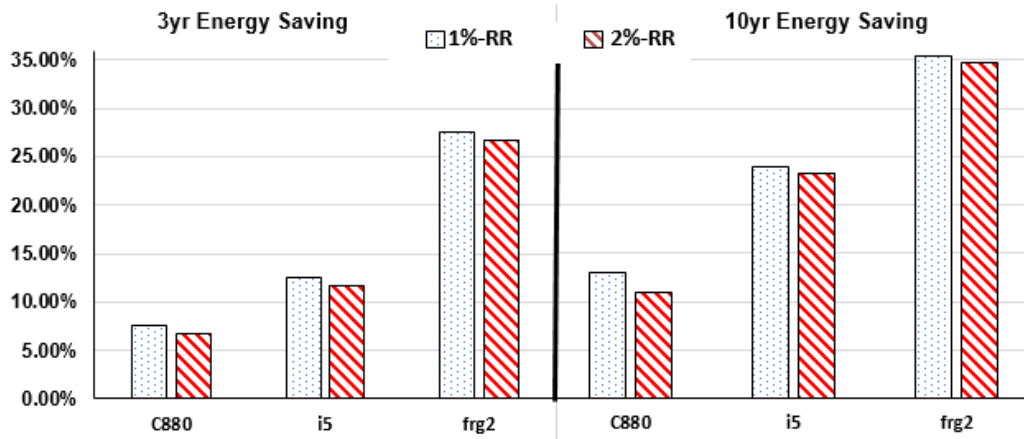


Figure 26: Percent energy savings relative to Baseline. ERT=1% and ERT=2% depicted for benchmark circuits.

Table 6: The minimum switching intervals obtained by RR for ERT=1% and ERT=2%

<b>Benchmarks</b>	ERT=1%	ERT=2%
<b>C880</b>	3.61 hrs	192 hrs
<b>i5</b>	0.25 hrs	9.6 hrs
<b>frg2</b>	3 hrs	120 hrs

Table 7: Initial Time Area/Energy Overheads with (n = 2) at Nominal Voltage

<b>Benchmarks</b>	No. of CGs	AO for p = 5%	AO for p = 10%	EO for p = 10%
<b>C880</b>	14	27.43%	34.18%	8.90%
<b>i5</b>	24	14.13%	18.18%	0.59%
<b>frg2</b>	42	20.86%	25.53%	7.15%

## CHAPTER SEVEN: CONCLUSION

The topology by which STs are arranged within a circuit can have dramatic impacts on the aging behavior of the integrated ST itself, which in turn causes a range of delay increases resulting in the observed performance reduction. Thus, a comprehensive study is required to offer the preferred ST arrangement. This necessity has been addressed in this thesis.

Furthermore, even though technology scaling has provided billions of transistors on a single chip, however the number of transistors which can be turned on simultaneously are limited to maintain the temperature of the chip within an acceptable range. The area of the chip that cannot be used during the circuit operation due to this so-called power wall constraint is referred as the dark silicon effect [79]. In this thesis, the dark silicon effect has inspired us to allocate the unused space to reduce the aging effect in the critical region of the circuit that determines aging-related degradation. This in turn saves significant energy while avoiding timing violation exposures.

### Technical Summary

To simulate the efficiency of the proposed techniques, the HSPICE tool [80] was selected as the circuit simulator. A very comprehensive document published by Synopsys [80] was used as a reference for determining the circuit's parameter over its lifetime. In addition, the Nangate 45nm Open Cell Library from Arizona State University was utilized to identify the transistor parameters. To assess the impact of aging on the ST arrangement and benchmarks, the MOSRA model commands were examined including final reliability test time to use in post-stress

simulation phase (RelTotalTime), time point of the first post-stress simulation (RelStartTime), post-stress simulation phases until it achieves the RelTotalTime (RelStep), and reliability model mode selection (RelMode).

We implement three different power-gating scenarios in order to investigate the impact of BTI on each of them. In the *Header-based ST (HST)*, we insert a PMOS ST to create virtual  $V_{DD}$ . Over the design and analysis of the impact of aging on the ST arrangement, the following technical insights were observed:

- One advantage of an HST arrangement is that PMOS transistor exhibits less leakage current than NMOS transistor of equivalent size.
- The NBTI effect elevates  $V_{th}$  over time and makes PMOS transistor even less leaky.
- The disadvantage of an HST arrangement is that PMOS has lower drive current than NMOS of a same size. As a result, a HST implementation usually consumes more area than a *Footer-based ST (FST)* implementation.
- The advantage of FST is its high drive current and hence smaller area for equivalent performance.
- However, NMOS is leakier than PMOS and application designs become more sensitive to ground noise on the virtual ground coupled through the FST.
- The NMOS ST also suffers from PBTI in active mode which imposes additive performance loss.
- However, the performance loss of HST and FST circuits is not equal since PMOS ST experiences more dramatic aging effects when it is used in an HST structure in compare

to NMOS ST in a FST design. Consequently, HST and FST designs both impact the logic network performance in a different way.

HFST takes advantage of both HST and FST in its implementation and bears a smaller amount of leakage current.

RR technique inspired by dark silicon concept deploys a simple shadow latch based timing sensor to examine the BTI impact throughout the lifetime operation of the circuit. The output data is sampled in two different points in time whereby the earlier sample is stored in the main latch while the latter sample is captured by the shadow latch operating with a delayed clock signal. Thus, the aging-induced timing violation can be simply detected by a comparison operation using a simple *XOR* logic gate. By detecting any timing violation in the circuit, an error signal is generated to trigger the feedback device controller for compensating the aging effect. This reactive function block, removes the stress condition in the currently active logic domain by putting it on the sleep mode while another unaged identical critical logic instance remodeled using *CPRT* is activated with a round-robin pattern to continue the function of the aged instance. Finally, an extendable technique to extract, remodel, and merge selectively replicated critical paths is demonstrated within existing EDA design flows.

#### Trading Area for Energy

RR provides an adaptive resource management technique for anti-aging using a sleep interval to enable BTI recovery. This autonomous selection behavior alleviates the need for any accurate aging modeling as actual circuit degradation is determined using actual runtime inputs. The proposed remodeling can be extended to enable self-selection and runtime competition

among logic domains in the presence of other noise sources such as process variation, temperature and voltage variations, and soft-errors. The favorable energy savings as high as 35.3% using RR are obtained due to reduction of operating voltage through autonomous adaptation of switching interval.

### Technical Insights Gained

By analysis the aging effect on ST arrangement scenarios, we observed that:

- FST arrangements can be preferred to minimize degradation of delay based on Figure 17 and Figure 18,
- HFST arrangements are seen to incur increased power consumption according to Table 5 and more area penalty according to Figure 14, yet Figure 15, Figure 16, Figure 17 and Figure 18 show HFST performs comparably to FST in terms of both  $V_{th}$  shift and delay degradation according to Table 4,
- The impact of the electric field between inputs and ground is not a significant influence on aging degradation between Figure 19 and Figure 20,
- HFST arrangements are seen to only slightly reduce ST  $V_{th}$  shift compared to HST in Figure 16 and Figure 17,
- Based on Figure 14, since HST has less leakage then the benefit of HFST may not be justified, and
- Area penalty of FST may provide a practical advantage for manufacturing layout while having less aging due to decreased impact of PBTI compared to NBTI.



The RR technique trades the area to save more energy while alleviate the aging effect. The following technical insights were observed while we were working on the proposed RR methodology:

- The autonomous resource management provided by RR reduces the delay degradation by a factor of 3.32-fold as compared to an uncompensated design.
- Reduced guardbands due to RR enables energy savings as high as 35.3% and 34.6% for `frg2` with ERT of 1% and 2% respectively over 10 years.
- The area overhead incurred to equip `c880` benchmark with the RR is 27.43% if we consider the top 5% of the path length distribution for aging mitigation.

### Future Works

An enhancement is to apply the proactive aging mitigation technique in which the computation workload of the critical or near critical path is transferred to one of the selected replica paths from the pool of identical paths at the end of considered interval. Essentially, this interval is estimated at design-time to determine the tolerable aging ratio in the circuit before the timing violation occurs. Then, the advantages and disadvantages of both proposed proactive and reactive aging mitigation techniques will be elaborated and the desired solution will be offered.

**APPENDIX A: HSPICE CODE FOR BASIC INVERTER CHAIN**  
**RELIABILITY ASSESSMENT**

```

*****
*****
**
**
**                               inv-100k-Basic.sp
**
*****
*****
*****
** Authors: Navid Khoshavi
** Email: navid.khoshavi@knights.ucf.edu
**Inv-100k
.inc "NangateOpenCellLibrary_supply.sp"
.inc "hybridmosra.lib"

* include transistor models
.LIB "_45nm_nominal_bulkCMOS.pm" CMOS_MODELS
.GLOBAL vdd
.param vddbase = 1.1
.param vdd='1*vddbase'
.param wpbase=630e-9
.param WpG='100*wpbase'
+ delay=100p
.TEMP 25

* define supply
vdd vdd 0 'vdd'

** drain gate source
.subckt INV a zn vvdd
m_i_1 zn a vvdd vvdd PMOS_1 L=50e-9 W=630e-9
m_i_0 zn a 0 0 NMOS_1 L=50e-9 W=415e-9
.ends INV
** End of subcircuit definition.

xinv1 in out1 vdd INV
xinv2 out1 out2 vdd INV
xinv3 out2 out3 vdd INV
xinv4 out3 out4 vdd INV
xinv5 out4 out5 vdd INV
xinv6 out5 out6 vdd INV
xinv7 out6 out7 vdd INV
xinv8 out7 out8 vdd INV
xinv9 out8 out9 vdd INV
xinv10 out9 out10 vdd INV
xinv11 out10 out11 vdd INV
xinv12 out11 out12 vdd INV
xinv13 out12 out13 vdd INV
xinv14 out13 out14 vdd INV
xinv15 out14 out15 vdd INV
xinv16 out15 out16 vdd INV
xinv17 out16 out17 vdd INV
xinv18 out17 out18 vdd INV
xinv19 out18 out19 vdd INV
xinv20 out19 out20 vdd INV

```

```

xinv21 out20 out21 vdd INV
xinv22 out21 out22 vdd INV
xinv23 out22 out23 vdd INV
xinv24 out23 out24 vdd INV
xinv25 out24 out25 vdd INV
xinv26 out25 out26 vdd INV
xinv27 out26 out27 vdd INV
xinv28 out27 out28 vdd INV
xinv29 out28 out29 vdd INV
xinv30 out29 out30 vdd INV
xinv31 out30 out31 vdd INV
xinv32 out31 out32 vdd INV
xinv33 out32 out33 vdd INV
xinv34 out33 out34 vdd INV
xinv35 out34 out35 vdd INV
xinv36 out35 out36 vdd INV
xinv37 out36 out37 vdd INV
xinv38 out37 out38 vdd INV
xinv39 out38 out39 vdd INV
xinv40 out39 out40 vdd INV
xinv41 out40 out41 vdd INV
xinv42 out41 out42 vdd INV
xinv43 out42 out43 vdd INV
xinv44 out43 out44 vdd INV
xinv45 out44 out45 vdd INV
xinv46 out45 out46 vdd INV
xinv47 out46 out47 vdd INV
xinv48 out47 out48 vdd INV
xinv49 out48 baseout vdd INV

```

*\* Load capacitance*

C0 baseout 0 10fF

*\*\*\*\*\* Reliability Analysis \*\*\*\*\**

**.model** p1 pmos level=54 version=4.5

**.model** n1 nmos level=54 version=4.5

**.appendmodel** p1\_ra mosra PMOS\_1 pmos

**.appendmodel** n1\_ra mosra NMOS\_1 nmos

**.mosra** reltotaltime='(10\*365\*24\*60\*60)'

+RelStep='365\*24\*60\*60'

+agingstart=1n agingstop=0.1ms

+RelMode=0

*\*-----Stimuli*

Vin in 0 pulse(vdd 0 1n 0 0 5000ns 10000ns)

*\*-----*

**.tran** 10p 0.1ms

*\*\*\*\*\* Measure delays\*\*\*\*\**

**.MEASURE** TRAN tpHL1 trig V(in) val='vdd/2' TD=10ns fall=1 targ V(baseout)  
val='vdd/2' rise=1

**.options** post=0

**.options** ingold=2 nomod numdgt=2 measdgt=5 runlvl=1 NOWARN statfl=1

**.option** radegoutput=csv

**.END**

**APPENDIX B: HSPICE CODE FOR INVERTER CHAIN WITH FOOTER**  
**SLEEP TRANSISTOR RELIABILITY ASSESSMENT**

```

*****
*****
**
**
**
**
*****
*****
*****
** Authors: Navid Khoshavi
** Email: navid.khoshavi@knights.ucf.edu

**Inv-100k-F
.inc "NangateOpenCellLibrary_supply.sp"
.inc "hybridmosra.lib"

* include transistor models
.LIB "_45nm_nominal_bulkCMOS.pm" CMOS_MODELS
.GLOBAL vdd
.param vddbase = 1.1
.param vdd='1*vddbase'
.param wpbase=630e-9
.param wnbase=415e-9
.param WpG='100*wpbase'
.param WnG='100*wnbase'
+ delay=100p
.TEMP 25

* define supply
vdd vdd 0 'vdd'

** drain gate source
.subckt INV a zn vvss vdd
m_i_1 zn a vdd vdd PMOS_1 L=50e-9 W=630e-9
m_i_0 zn a vvss vvss NMOS_1 L=50e-9 W=415e-9
.ends INV
** End of subcircuit definition.

xinv1 in out1 vvss vdd INV
xinv2 out1 out2 vvss vdd INV
xinv3 out2 out3 vvss vdd INV
xinv4 out3 out4 vvss vdd INV
xinv5 out4 out5 vvss vdd INV
xinv6 out5 out6 vvss vdd INV
xinv7 out6 out7 vvss vdd INV
xinv8 out7 out8 vvss vdd INV
xinv9 out8 out9 vvss vdd INV
xinv10 out9 out10 vvss vdd INV
xinv11 out10 out11 vvss vdd INV
xinv12 out11 out12 vvss vdd INV
xinv13 out12 out13 vvss vdd INV
xinv14 out13 out14 vvss vdd INV
xinv15 out14 out15 vvss vdd INV
xinv16 out15 out16 vvss vdd INV
xinv17 out16 out17 vvss vdd INV

```

```

xinv18 out17 out18 vvss vdd INV
xinv19 out18 out19 vvss vdd INV
xinv20 out19 out20 vvss vdd INV
xinv21 out20 out21 vvss vdd INV
xinv22 out21 out22 vvss vdd INV
xinv23 out22 out23 vvss vdd INV
xinv24 out23 out24 vvss vdd INV
xinv25 out24 out25 vvss vdd INV
xinv26 out25 out26 vvss vdd INV
xinv27 out26 out27 vvss vdd INV
xinv28 out27 out28 vvss vdd INV
xinv29 out28 out29 vvss vdd INV
xinv30 out29 out30 vvss vdd INV
xinv31 out30 out31 vvss vdd INV
xinv32 out31 out32 vvss vdd INV
xinv33 out32 out33 vvss vdd INV
xinv34 out33 out34 vvss vdd INV
xinv35 out34 out35 vvss vdd INV
xinv36 out35 out36 vvss vdd INV
xinv37 out36 out37 vvss vdd INV
xinv38 out37 out38 vvss vdd INV
xinv39 out38 out39 vvss vdd INV
xinv40 out39 out40 vvss vdd INV
xinv41 out40 out41 vvss vdd INV
xinv42 out41 out42 vvss vdd INV
xinv43 out42 out43 vvss vdd INV
xinv44 out43 out44 vvss vdd INV
xinv45 out44 out45 vvss vdd INV
xinv46 out45 out46 vvss vdd INV
xinv47 out46 out47 vvss vdd INV
xinv48 out47 out48 vvss vdd INV
xinv49 out48 baseout vvss vdd INV

MPower1 vvss nst 0 0 NMOS_1 L=50e-9 W=WnG

* Load capacitance
C0 baseout 0 10fF

***** Reliability Analysis *****
.model p1 pmos level=54 version=4.5
.model n1 nmos level=54 version=4.5
.appendmodel p1_ra mosra PMOS_1 pmos
.appendmodel n1_ra mosra NMOS_1 nmos
.mosra reltotaltime='(0.7*365*24*60*60)'
+RelStep='0.7*365*24*60*60'
+agingstart=1n agingstop=0.1ms
+RelMode=0

.option radegfile = 'inv-100k-F.radeg0'
*-----Stimuli
Vin in 0 pulse(vdd 0 1n 0 0 5000ns 10000ns)

Vnst nst 0 pulse(0 0 0 0 0 0.1ms 0.1m)
*-----

```

```

.tran 10p 0.1ms
***** Measure delays*****
.MEASURE TRAN tpHL1 trig V(in) val='vdd/2' TD=10ns fall=1 targ V(baseout)
val='vdd/2' rise=1

.options post=0
.options ingold=2 nomod numdgt=2 measdgt=5 runlvl=1 NOWARN statfl=1
.option radegoutput=csv

* after 0.7 of year
.alter
.mosra reltotaltime='(0.3*365*24*60*60)' simmode=3
+RelStep='0.3*365*24*60*60'
+agingstart=1n agingstop=0.1ms
+RelMode=0
*%0.001 second with alter command
*sleep signals set here
*alter sleep signal only
Vnst nst 0 pulse(vdd vdd 0 0 0 0.1ms 0.1m)
*Vpst pst vdd 0

* after 1 year
.alter
.mosra reltotaltime='(0.7*365*24*60*60)' simmode=3
+RelStep='0.7*365*24*60*60'
+agingstart=1n agingstop=0.1ms
+RelMode=0
Vnst nst 0 pulse(0 0 0 0 0 0.1ms 0.1m)

.alter
.mosra reltotaltime='(0.3*365*24*60*60)' simmode=3
+RelStep='0.3*365*24*60*60'
+agingstart=1n agingstop=0.1ms
+RelMode=0
Vnst nst 0 pulse(vdd vdd 0 0 0 0.1ms 0.1m)

* after 2 year
.alter
.mosra reltotaltime='(0.7*365*24*60*60)' simmode=3
+RelStep='0.7*365*24*60*60'
+agingstart=1n agingstop=0.1ms
+RelMode=0
Vnst nst 0 pulse(0 0 0 0 0 0.1ms 0.1m)

.alter
.mosra reltotaltime='(0.3*365*24*60*60)' simmode=3
+RelStep='0.3*365*24*60*60'
+agingstart=1n agingstop=0.1ms
+RelMode=0
Vnst nst 0 pulse(vdd vdd 0 0 0 0.1ms 0.1m)

* after 3 year
.alter

```



```
.mosra reltotaltime='(0.7*365*24*60*60)' simmode=3
+RelStep='0.7*365*24*60*60'
+agingstart=1n agingstop=0.1ms
+RelMode=0
Vnst nst 0 pulse(0 0 0 0 0 0.1ms 0.1m)
```

```
.alter
.mosra reltotaltime='(0.3*365*24*60*60)' simmode=3
+RelStep='0.3*365*24*60*60'
+agingstart=1n agingstop=0.1ms
+RelMode=0
Vnst nst 0 pulse(vdd vdd 0 0 0 0.1ms 0.1m)
```

\* after 4 year

```
.alter
.mosra reltotaltime='(0.7*365*24*60*60)' simmode=3
+RelStep='0.7*365*24*60*60'
+agingstart=1n agingstop=0.1ms
+RelMode=0
Vnst nst 0 pulse(0 0 0 0 0 0.1ms 0.1m)
```

```
.alter
.mosra reltotaltime='(0.3*365*24*60*60)' simmode=3
+RelStep='0.3*365*24*60*60'
+agingstart=1n agingstop=0.1ms
+RelMode=0
Vnst nst 0 pulse(vdd vdd 0 0 0 0.1ms 0.1m)
```

\* after 5 year

```
.alter
.mosra reltotaltime='(0.7*365*24*60*60)' simmode=3
+RelStep='0.7*365*24*60*60'
+agingstart=1n agingstop=0.1ms
+RelMode=0
Vnst nst 0 pulse(0 0 0 0 0 0.1ms 0.1m)
```

```
.alter
.mosra reltotaltime='(0.3*365*24*60*60)' simmode=3
+RelStep='0.3*365*24*60*60'
+agingstart=1n agingstop=0.1ms
+RelMode=0
Vnst nst 0 pulse(vdd vdd 0 0 0 0.1ms 0.1m)
```

\* after 6 year

```
.alter
.mosra reltotaltime='(0.7*365*24*60*60)' simmode=3
+RelStep='0.7*365*24*60*60'
+agingstart=1n agingstop=0.1ms
+RelMode=0
Vnst nst 0 pulse(0 0 0 0 0 0.1ms 0.1m)
```

```
.alter
```

```
.mosra reltotaltime='(0.3*365*24*60*60)' simmode=3
+RelStep='0.3*365*24*60*60'
+agingstart=1n agingstop=0.1ms
+RelMode=0
Vnst nst 0 pulse(vdd vdd 0 0 0 0.1ms 0.1m)
```

\* after 7 year

```
.alter
.mosra reltotaltime='(0.7*365*24*60*60)' simmode=3
+RelStep='0.7*365*24*60*60'
+agingstart=1n agingstop=0.1ms
+RelMode=0
Vnst nst 0 pulse(0 0 0 0 0 0.1ms 0.1m)
```

```
.alter
.mosra reltotaltime='(0.3*365*24*60*60)' simmode=3
+RelStep='0.3*365*24*60*60'
+agingstart=1n agingstop=0.1ms
+RelMode=0
Vnst nst 0 pulse(vdd vdd 0 0 0 0.1ms 0.1m)
```

\* after 8 year

```
.alter
.mosra reltotaltime='(0.7*365*24*60*60)' simmode=3
+RelStep='0.7*365*24*60*60'
+agingstart=1n agingstop=0.1ms
+RelMode=0
Vnst nst 0 pulse(0 0 0 0 0 0.1ms 0.1m)
```

```
.alter
.mosra reltotaltime='(0.3*365*24*60*60)' simmode=3
+RelStep='0.3*365*24*60*60'
+agingstart=1n agingstop=0.1ms
+RelMode=0
Vnst nst 0 pulse(vdd vdd 0 0 0 0.1ms 0.1m)
```

\* after 9 year

```
.alter
.mosra reltotaltime='(0.7*365*24*60*60)' simmode=3
+RelStep='0.7*365*24*60*60'
+agingstart=1n agingstop=0.1ms
+RelMode=0
Vnst nst 0 pulse(0 0 0 0 0 0.1ms 0.1m)
```

```
.alter
.mosra reltotaltime='(0.3*365*24*60*60)' simmode=3
+RelStep='0.3*365*24*60*60'
+agingstart=1n agingstop=0.1ms
+RelMode=0
Vnst nst 0 pulse(vdd vdd 0 0 0 0.1ms 0.1m)
```

```
.END
```

## **APPENDIX C: HSPICE CODE FOR I5 BENCHMARK IN RR METHOD**

```

*****
*****
**
**
**
**
*****
*****
*****
** Authors: Rizwan A Ashraf, Ahmad Alzahrani, Navid Khoshavi
** Email: navid.khoshavi@knights.ucf.edu
* Cell name: i5_CCP_N2_D0_P10

* include Nangate library
.inc "NangateOpenCellLibrary_supply.sp"
.inc "NangateOpenCellLibrary_ra.sp"

* include transistor models
.LIB "_45nm_nominal_bulkCMOS.pm" CMOS_MODELS

.param vdd =1.109
+ delay=100p
+ st_width=72.00000U
.TEMP 105

* define supply
vdd vdd 0 'vdd'

*sleep transistors
M_sleeptransistor_1 vdd_ccpn1 enable_ccp_n1 vdd vdd PMOS_VTL w=st_width
l=0.050000U
M_sleeptransistor_2 vdd_ccpn2 enable_ccp_n2 vdd vdd PMOS_VTL w=st_width
l=0.050000U

* Library name: NangateOpenCellLibrary
* Cell name: i5_CCP_N2_D0_P10
* View name: schematic
xu398_ccpn1 v16_5 v28_5 v151_6 n343_ccpn1 0 vdd_ccpn1 aoi21_x1
xu390_ccpn1 v16_6 v28_6 v151_7 n344_ccpn1 0 vdd_ccpn1 aoi21_x1
xu398_ccpn2 v16_5 v28_5 v151_6_ccpn2 n343_ccpn2 0 vdd_ccpn2 aoi21_x1
xu385_ccpn2 v16_7 v28_7 v151_8_ccpn2 n345_ccpn2 0 vdd_ccpn2 aoi21_x1
xu385_ccpn1 v16_7 v28_7 v151_8 n345_ccpn1 0 vdd_ccpn1 aoi21_x1
xu390_ccpn2 v16_6 v28_6 v151_7_ccpn2 n344_ccpn2 0 vdd_ccpn2 aoi21_x1
xu392_ccpn1 v16_2 v28_2 v151_3 n352_ccpn1 0 vdd_ccpn1 aoi21_x1
xu386_ccpn1 v16_3 v28_3 v151_4 n353_ccpn1 0 vdd_ccpn1 aoi21_x1
xu401_ccpn1 v16_1 v28_1 v151_2 n351_ccpn1 0 vdd_ccpn1 aoi21_x1
xu401_ccpn2 v16_1 v28_1 v151_2_ccpn2 n351_ccpn2 0 vdd_ccpn2 aoi21_x1
xu392_ccpn2 v16_2 v28_2 v151_3_ccpn2 n352_ccpn2 0 vdd_ccpn2 aoi21_x1
xu382_ccpn2 v103_1 v106_1 v151_8_ccpn2 n354_ccpn2 0 vdd_ccpn2 aoi21_x1
xu382_ccpn1 v103_1 v106_1 v151_8 n354_ccpn1 0 vdd_ccpn1 aoi21_x1
xu386_ccpn2 v16_3 v28_3 v151_4_ccpn2 n353_ccpn2 0 vdd_ccpn2 aoi21_x1
xu377_ccpn1 v103_3 v106_3 v167_0 n356_ccpn1 0 vdd_ccpn1 aoi21_x1
xu377_ccpn2 v103_3 v106_3 v167_0_ccpn2 n356_ccpn2 0 vdd_ccpn2 aoi21_x1
xu381_ccpn1 v128_1 v132_1 v183_0 n360_ccpn1 0 vdd_ccpn1 aoi21_x1
xu375_ccpn1 v128_2 v132_2 v199_0 n361_ccpn1 0 vdd_ccpn1 aoi21_x1

```

```

xu381_ccpn2 v128_1 v132_1 v183_0_ccpn2 n360_ccpn2 0 vdd_ccpn2 aoi21_x1
xu375_ccpn2 v128_2 v132_2 v199_0_ccpn2 n361_ccpn2 0 vdd_ccpn2 aoi21_x1
xu374_ccpn2 v128_3 v132_3 v133_0 n362_ccpn2 0 vdd_ccpn2 aoi21_x1
xu374_ccpn1 v128_3 v132_3 v133_0 n362_ccpn1 0 vdd_ccpn1 aoi21_x1
xu379_ccpn1 v103_2 v106_2 v151_12 n355_ccpn1 0 vdd_ccpn1 aoi21_x1
xu379_ccpn2 v103_2 v106_2 v151_12_ccpn2 n355_ccpn2 0 vdd_ccpn2 aoi21_x1
xu423 v16_11 v28_11 v151_12 n350 0 vdd aoi21_x1
xu449 v16_10 v28_10 v151_11 n349 0 vdd aoi21_x1
xu466 v16_9 v28_9 v151_10 n342 0 vdd aoi21_x1
xu445 v40_6 v52_6 v167_7 n329 0 vdd aoi21_x1
xu421 v40_7 v52_7 v167_8 n330 0 vdd aoi21_x1
xu493 v40_5 v52_5 v167_6 n328 0 vdd aoi21_x1
xu490 v64_1 v76_1 v183_2 n321 0 vdd aoi21_x1
xu417 v64_3 v76_3 v183_4 n323 0 vdd aoi21_x1
xu408 v115_1 v118_1 v183_8 n324 0 vdd aoi21_x1
xu439 v64_2 v76_2 v183_3 n322 0 vdd aoi21_x1
xu437 v64_6 v76_6 v183_7 n314 0 vdd aoi21_x1
xu416 v64_7 v76_7 v183_8 n315 0 vdd aoi21_x1
xu487 v64_5 v76_5 v183_6 n313 0 vdd aoi21_x1
xu406 v115_2 v118_2 v183_12 n325 0 vdd aoi21_x1
xu484 v64_13 v76_13 v183_14 n316 0 vdd aoi21_x1
xu414 v64_15 v76_15 v199_0 n318 0 vdd aoi21_x1
xu404 v115_3 v118_3 v199_0 n326 0 vdd aoi21_x1
xu433 v64_14 v76_14 v183_15 n317 0 vdd aoi21_x1
xu435 v64_10 v76_10 v183_11 n319 0 vdd aoi21_x1
xu454 v64_9 v76_9 v183_10 n312 0 vdd aoi21_x1
xu415 v64_11 v76_11 v183_12 n320 0 vdd aoi21_x1
xu481 v88_1 v100_1 v199_2 n306 0 vdd aoi21_x1
xu412 v88_3 v100_3 v199_4 n308 0 vdd aoi21_x1
xu407 v121_1 v124_1 v199_8 n309 0 vdd aoi21_x1
xu431 v88_2 v100_2 v199_3 n307 0 vdd aoi21_x1
xu429 v88_6 v100_6 v199_7 n299 0 vdd aoi21_x1
xu411 v88_7 v100_7 v199_8 n300 0 vdd aoi21_x1
xu478 v88_5 v100_5 v199_6 n298 0 vdd aoi21_x1
xu427 v88_10 v100_10 v199_11 n304 0 vdd aoi21_x1
xu410 v88_11 v100_11 v199_12 n305 0 vdd aoi21_x1
xu475 v88_9 v100_9 v199_10 n297 0 vdd aoi21_x1
xu403 v121_3 v133_0 v124_3 n311 0 vdd aoi21_x1
xu425 v88_14 v100_14 v199_15 n302 0 vdd aoi21_x1
xu472 v88_13 v100_13 v199_14 n301 0 vdd aoi21_x1
xu409 v88_15 v100_15 v133_0 n303 0 vdd aoi21_x1
xu451 v2_1 v4_1 v151_0 n358 0 vdd aoi21_x1
xu424 v128_0 v132_0 v167_0 n359 0 vdd aoi21_x1
xu469 v2_0 v4_0 v135_1 n357 0 vdd aoi21_x1
xu447 v16_14 v28_14 v151_15 n347 0 vdd aoi21_x1
xu463 v16_13 v28_13 v151_14 n346 0 vdd aoi21_x1
xu422 v16_15 v28_15 v167_0 n348 0 vdd aoi21_x1
xu443 v40_10 v52_10 v167_11 n334 0 vdd aoi21_x1
xu420 v40_11 v52_11 v167_12 n335 0 vdd aoi21_x1
xu460 v40_9 v52_9 v167_10 n327 0 vdd aoi21_x1
xu457 v40_13 v52_13 v167_14 n331 0 vdd aoi21_x1
xu419 v40_15 v52_15 v183_0 n333 0 vdd aoi21_x1
xu376 v109_3 v112_3 v183_0 n341 0 vdd aoi21_x1
xu441 v40_14 v52_14 v167_15 n332 0 vdd aoi21_x1

```

```

xu378 v109_2 v112_2 v167_12 n340 0 vdd ao121_x1
xu380 v109_1 v112_1 v167_8 n339 0 vdd ao121_x1
xu388 v40_2 v52_2 v167_3 n337 0 vdd ao121_x1
xu395 v40_1 v52_1 v167_2 n336 0 vdd ao121_x1
xu383 v40_3 v52_3 v167_4 n338 0 vdd ao121_x1
xu405 v121_2 v124_2 v199_12 n310 0 vdd ao121_x1
xu399_ccpn1 n344_ccpn1 v151_6 0 vdd_ccpn1 inv_x1
xu397_ccpn1 n343_ccpn1 v151_5 0 vdd_ccpn1 inv_x1
xu397_ccpn2 n343_ccpn2 v151_5_ccpn2 0 vdd_ccpn2 inv_x1
xu399_ccpn2 n344_ccpn2 v151_6_ccpn2 0 vdd_ccpn2 inv_x1
xu391_ccpn2 n345_ccpn2 v151_7_ccpn2 0 vdd_ccpn2 inv_x1
xu391_ccpn1 n345_ccpn1 v151_7 0 vdd_ccpn1 inv_x1
xu400_ccpn1 n351_ccpn1 v151_1 0 vdd_ccpn1 inv_x1
xu402_ccpn1 n352_ccpn1 v151_2 0 vdd_ccpn1 inv_x1
xu393_ccpn1 n353_ccpn1 v151_3 0 vdd_ccpn1 inv_x1
xu400_ccpn2 n351_ccpn2 v151_1_ccpn2 0 vdd_ccpn2 inv_x1
xu402_ccpn2 n352_ccpn2 v151_2_ccpn2 0 vdd_ccpn2 inv_x1
xu393_ccpn2 n353_ccpn2 v151_3_ccpn2 0 vdd_ccpn2 inv_x1
xu387_ccpn2 n354_ccpn2 v151_4_ccpn2 0 vdd_ccpn2 inv_x1
xu387_ccpn1 n354_ccpn1 v151_4 0 vdd_ccpn1 inv_x1
xu365_ccpn1 n360_ccpn1 v167_0 0 vdd_ccpn1 inv_x1
xu367_ccpn1 n356_ccpn1 v151_12 0 vdd_ccpn1 inv_x1
xu367_ccpn2 n356_ccpn2 v151_12_ccpn2 0 vdd_ccpn2 inv_x1
xu365_ccpn2 n360_ccpn2 v167_0_ccpn2 0 vdd_ccpn2 inv_x1
xu363_ccpn1 n362_ccpn1 v199_0 0 vdd_ccpn1 inv_x1
xu364_ccpn1 n361_ccpn1 v183_0 0 vdd_ccpn1 inv_x1
xu364_ccpn2 n361_ccpn2 v183_0_ccpn2 0 vdd_ccpn2 inv_x1
xu363_ccpn2 n362_ccpn2 v199_0_ccpn2 0 vdd_ccpn2 inv_x1
xu369_ccpn1 n355_ccpn1 v151_8 0 vdd_ccpn1 inv_x1
xu369_ccpn2 n355_ccpn2 v151_8_ccpn2 0 vdd_ccpn2 inv_x1
xu467 n349 v151_10 0 vdd inv_x1
xu465 n342 v151_9 0 vdd inv_x1
xu450 n350 v151_11 0 vdd inv_x1
xu492 n328 v167_5 0 vdd inv_x1
xu494 n329 v167_6 0 vdd inv_x1
xu446 n330 v167_7 0 vdd inv_x1
xu489 n321 v183_1 0 vdd inv_x1
xu491 n322 v183_2 0 vdd inv_x1
xu440 n323 v183_3 0 vdd inv_x1
xu418 n324 v183_4 0 vdd inv_x1
xu486 n313 v183_5 0 vdd inv_x1
xu488 n314 v183_6 0 vdd inv_x1
xu438 n315 v183_7 0 vdd inv_x1
xu373 n325 v183_8 0 vdd inv_x1
xu485 n317 v183_14 0 vdd inv_x1
xu483 n316 v183_13 0 vdd inv_x1
xu434 n318 v183_15 0 vdd inv_x1
xu371 n326 v183_12 0 vdd inv_x1
xu436 n320 v183_11 0 vdd inv_x1
xu455 n319 v183_10 0 vdd inv_x1
xu453 n312 v183_9 0 vdd inv_x1
xu480 n306 v199_1 0 vdd inv_x1
xu482 n307 v199_2 0 vdd inv_x1
xu432 n308 v199_3 0 vdd inv_x1

```

```

xu413 n309 v199_4 0 vdd inv_x1
xu477 n298 v199_5 0 vdd inv_x1
xu479 n299 v199_6 0 vdd inv_x1
xu430 n300 v199_7 0 vdd inv_x1
xu474 n297 v199_9 0 vdd inv_x1
xu476 n304 v199_10 0 vdd inv_x1
xu428 n305 v199_11 0 vdd inv_x1
xu370 n311 v199_12 0 vdd inv_x1
xu426 n303 v199_15 0 vdd inv_x1
xu473 n302 v199_14 0 vdd inv_x1
xu471 n301 v199_13 0 vdd inv_x1
xu468 n357 v135_0 0 vdd inv_x1
xu470 n358 v135_1 0 vdd inv_x1
xu452 n359 v151_0 0 vdd inv_x1
xu448 n348 v151_15 0 vdd inv_x1
xu464 n347 v151_14 0 vdd inv_x1
xu462 n346 v151_13 0 vdd inv_x1
xu459 n327 v167_9 0 vdd inv_x1
xu461 n334 v167_10 0 vdd inv_x1
xu444 n335 v167_11 0 vdd inv_x1
xu456 n331 v167_13 0 vdd inv_x1
xu458 n332 v167_14 0 vdd inv_x1
xu442 n333 v167_15 0 vdd inv_x1
xu366 n341 v167_12 0 vdd inv_x1
xu368 n340 v167_8 0 vdd inv_x1
xu384 n339 v167_4 0 vdd inv_x1
xu389 n338 v167_3 0 vdd inv_x1
xu396 n337 v167_2 0 vdd inv_x1
xu394 n336 v167_1 0 vdd inv_x1
xu372 n310 v199_8 0 vdd inv_x1

```

\* load at outputs

```

c1 V135_0 0 1.14029e-15
c2 V135_1 0 1.14029e-15
c3 V151_1 0 1.14029e-15
c302 V151_1_ccpn2 0 1.14029e-15
c4 V151_2 0 1.14029e-15
c402 V151_2_ccpn2 0 1.14029e-15
c5 V151_3 0 1.14029e-15
c6 V151_5 0 1.14029e-15
c602 V151_5_ccpn2 0 1.14029e-15
c7 V151_6 0 1.14029e-15
c8 V151_7 0 1.14029e-15
c9 V151_9 0 1.14029e-15
c10 V151_10 0 1.14029e-15
c11 V151_11 0 1.14029e-15
c12 V151_13 0 1.14029e-15
c13 V151_14 0 1.14029e-15
c14 V151_15 0 1.14029e-15
c15 V167_1 0 1.14029e-15
c16 V167_2 0 1.14029e-15
c17 V167_3 0 1.14029e-15
c18 V167_5 0 1.14029e-15
c19 V167_6 0 1.14029e-15

```

```

c20 V167_7 0 1.14029e-15
c21 V167_9 0 1.14029e-15
c22 V167_10 0 1.14029e-15
c23 V167_11 0 1.14029e-15
c24 V167_13 0 1.14029e-15
c25 V167_14 0 1.14029e-15
c26 V167_15 0 1.14029e-15
c27 V183_1 0 1.14029e-15
c28 V183_2 0 1.14029e-15
c29 V183_3 0 1.14029e-15
c30 V183_5 0 1.14029e-15
c31 V183_6 0 1.14029e-15
c32 V183_7 0 1.14029e-15
c33 V183_9 0 1.14029e-15
c34 V183_10 0 1.14029e-15
c35 V183_11 0 1.14029e-15
c36 V183_13 0 1.14029e-15
c37 V183_14 0 1.14029e-15
c38 V183_15 0 1.14029e-15
c39 V199_1 0 1.14029e-15
c40 V199_2 0 1.14029e-15
c41 V199_3 0 1.14029e-15
c42 V199_5 0 1.14029e-15
c43 V199_6 0 1.14029e-15
c44 V199_7 0 1.14029e-15
c45 V199_9 0 1.14029e-15
c46 V199_10 0 1.14029e-15
c47 V199_11 0 1.14029e-15
c48 V199_13 0 1.14029e-15
c49 V199_14 0 1.14029e-15
c50 V199_15 0 1.14029e-15
c51 V151_4 0 1.14029e-15
c52 V151_8 0 1.14029e-15
c53 V151_12 0 1.14029e-15
c54 V167_4 0 1.14029e-15
c55 V167_8 0 1.14029e-15
c56 V167_12 0 1.14029e-15
c57 V183_4 0 1.14029e-15
c58 V183_8 0 1.14029e-15
c59 V183_12 0 1.14029e-15
c60 V199_4 0 1.14029e-15
c61 V199_8 0 1.14029e-15
c62 V199_12 0 1.14029e-15
c63 V151_0 0 1.14029e-15
c64 V167_0 0 1.14029e-15
c65 V183_0 0 1.14029e-15
c66 V199_0 0 1.14029e-15

```

```

*mosra parameters
*Include mosra lib
.inc hybridmosra.lib

```

```

.appendmodel pl_ra mosra PMOS_VTL pmos

```



```

.appendmodel n1_ra mosra NMOS_VTL nmos

.mosra relttotaltime='900' simmode=3

.option radegfile = 'i5_CCP_N2_D0_P10.radeg95'

Venable_ccp_n1 enable_ccp_n1 0 0
Venable_ccp_n2 enable_ccp_n2 0 vdd

* input stimulus
.vec i5_org.vec

*transient analysis
.tran 5ps 10ns

* include measure stats
.inc measure_stats.sp

.MEASURE TRAN Icc INTEG I(vdd) FROM=6n TO=10n
.measure E_cct Param='-Icc*vdd'
.measure P_cct Param='E_cct/4n'

*.options post
.options ingold=2 nomod numdgt=10 measdgt=10 runlvl=3
.option ARTIST=2 PSF=2 WARN_SEP=1
.option SAMPLING_METHOD=SRS LIS_NEW=1

***** Start *****
.alter
.mosra relttotaltime='900' simmode=3

*sleep signals set here
Venable_ccp_n1 enable_ccp_n1 0 vdd
Venable_ccp_n2 enable_ccp_n2 0 0

.alter
.mosra relttotaltime='900' simmode=3

*sleep signals set here
Venable_ccp_n1 enable_ccp_n1 0 0
Venable_ccp_n2 enable_ccp_n2 0 vdd
*
*
*
***** end of one day *****

.END

```

## REFERENCES

- [1] R. A. Ashraf, A. Al-Zahrani, N. Khoshavi, R. Zand, S. Salehi, A. Roohi, *et al.*, "Reactive rejuvenation of CMOS logic paths using self-activating voltage domains," in *Circuits and Systems (ISCAS), 2015 IEEE International Symposium on*, 2015, pp. 2944-2947.
- [2] B. B. H. Calhoun, Y. Cao, X. Li, K. Mai, L. T. Pileggi, R. A. Rutenbar, *et al.*, "Digital circuit design challenges and opportunities in the era of nanoscale CMOS," *Proceedings of the IEEE*, vol. 96, pp. 343-365, 2008.
- [3] N. Miskov-Zivanov and D. Marculescu, "Multiple transient faults in combinational and sequential circuits: A systematic approach," *Computer-Aided Design of Integrated Circuits and Systems, IEEE Transactions on*, vol. 29, pp. 1614-1627, 2010.
- [4] L. Ratti, "Ionizing radiation effects in electronic devices and circuits," 2013.
- [5] R. C. Baumann, "Radiation-induced soft errors in advanced semiconductor technologies," *Device and Materials Reliability, IEEE Transactions on*, vol. 5, pp. 305-316, 2005.
- [6] S. Ganapathy, R. Canal, D. Alexandrescu, E. Costenaro, A. González, and A. Rubio, "A novel variation-tolerant 4T-DRAM cell with enhanced soft-error tolerance," in *Computer Design (ICCD), 2012 IEEE 30th International Conference on*, 2012, pp. 472-477.
- [7] M. Stanisavljević, A. Schmid, and Y. Leblebici, *Reliability of Nanoscale Circuits and Systems: Methodologies and Circuit Architectures*: Springer Science & Business Media, 2010.
- [8] C. Constantinescu, "Impact of intermittent faults on nanocomputing devices," in *DSN 2007 Workshop on Dependable and Secure Nanocomputing*, 2007.

- [9] Wikipedia. (2010). *Electromigration*. Available:  
<https://en.wikipedia.org/wiki/Electromigration>
- [10] C.-H. Ho, K. A. Jenkins, H. Ainspan, E. Ray, B. P. Linder, and P. Song, "Performance Degradation Analysis and Hot-Carrier Injection Impact on the Lifetime Prediction of Voltage Control Oscillator," *Electron Devices, IEEE Transactions on*, vol. 62, pp. 2148-2154, 2015.
- [11] A. Rahman, M. Agostinelli, P. Bai, G. Curello, H. Deshpande, W. Hafez, *et al.*, "Reliability studies of a 32nm System-on-Chip (SoC) platform technology with 2 nd generation high-k/metal gate transistors," in *Reliability Physics Symposium (IRPS), 2011 IEEE International*, 2011, pp. 5D. 3.1-5D. 3.6.
- [12] F. Oboril and M. B. Tahoori, "Cross-Layer Approaches for an Aging-Aware Design Space Exploration for Microprocessors," 2016.
- [13] T. Mak, "Is CMOS more reliable with scaling?," in *IEEE Int. On-Line Testing Workshop*, 2002.
- [14] J. P. Keane, "On-Chip Circuits for Characterizing Transistor Aging Mechanisms in Advanced CMOS Technologies," UNIVERSITY OF MINNESOTA, 2010.
- [15] K. Kang, S. P. Park, K. Roy, and M. A. Alam, "Estimation of statistical variation in temporal NBTI degradation and its impact on lifetime circuit performance," in *Computer-Aided Design, 2007. ICCAD 2007. IEEE/ACM International Conference on*, 2007, pp. 730-734.

- [16] D. Lorenz, M. Barke, and U. Schlichtmann, "Aging analysis at gate and macro cell level," in *Proceedings of the International Conference on Computer-Aided Design*, 2010, pp. 77-84.
- [17] K.-C. Wu and D. Marculescu, "Aging-aware timing analysis and optimization considering path sensitization," in *Design, Automation & Test in Europe Conference & Exhibition (DATE), 2011*, 2011, pp. 1-6.
- [18] M. Ebrahimi, F. Oboril, S. Kiamehr, and M. B. Tahoori, "Aging-aware logic synthesis," in *Proceedings of the International Conference on Computer-Aided Design*, 2013, pp. 61-68.
- [19] F. Firouzi, S. Kiamehr, M. Tahoori, and S. Nassif, "Incorporating the impacts of workload-dependent runtime variations into timing analysis," in *Proceedings of the Conference on Design, Automation and Test in Europe*, 2013, pp. 1022-1025.
- [20] S. Karapetyan and U. Schlichtmann, "Integrating aging aware timing analysis into a commercial STA tool," in *VLSI Design, Automation and Test (VLSI-DAT), 2015 International Symposium on*, 2015, pp. 1-4.
- [21] M. Ershov, S. Saxena, H. Karbasi, S. Winters, S. Minehane, J. Babcock, *et al.*, "Dynamic recovery of negative bias temperature instability in p-type metal–oxide–semiconductor field-effect transistors," *Applied physics letters*, vol. 83, pp. 1647-1649, 2003.
- [22] S. Rangan, N. Mielke, and E. Yeh, "Universal recovery behavior of negative bias temperature instability [PMOSFETs]," in *Electron Devices Meeting, 2003. IEDM'03 Technical Digest. IEEE International*, 2003, pp. 14.3. 1-14.3. 4.

- [23] V. Huard, M. Denais, and C. Parthasarathy, "NBTI degradation: From physical mechanisms to modelling," *Microelectronics Reliability*, vol. 46, pp. 1-23, 2006.
- [24] T. T.-H. Kim and Z. H. Kong, "Impact analysis of nbt/pbti on sram v min and design techniques for improved sram v min," *JSTS: Journal of Semiconductor Technology and Science*, vol. 13, pp. 87-97, 2013.
- [25] K. Sutaria, "Modeling and Simulation Tools for Aging Effects in Scaled CMOS Design," Arizona State University, 2015.
- [26] J. B. Velamala, K. Sutaria, T. Sato, and Y. Cao, "Physics matters: statistical aging prediction under trapping/detrapping," in *Proceedings of the 49th Annual Design Automation Conference*, 2012, pp. 139-144.
- [27] K. Sutaria, A. Ramkumar, R. Zhu, R. Rajveev, Y. Ma, and Y. Cao, "BTI-induced aging under random stress waveforms: Modeling, simulation and silicon Validation," in *Proceedings of the 51st Annual Design Automation Conference*, 2014, pp. 1-6.
- [28] B. Tudor, J. Wang, W. Liu, and H. Elhak, "MOS device aging analysis with HSPICE and CustomSim," *Synopsys, White Paper*, 2011.
- [29] M. Denais, V. Huard, C. Parthasarathy, G. Ribes, F. Perrier, N. Revil, *et al.*, "Interface trap generation and hole trapping under NBTI and PBTI in advanced CMOS technology with a 2-nm gate oxide," *Device and Materials Reliability, IEEE Transactions on*, vol. 4, pp. 715-722, 2004.
- [30] Y. Lu, L. Shang, H. Zhou, H. Zhu, F. Yang, and X. Zeng, "Statistical reliability analysis under process variation and aging effects," in *Proceedings of the 46th Annual Design Automation Conference*, 2009, pp. 514-519.

- [31] J. K. T.-H. K. Chris and H. Kim, "An On-Chip NBTI Sensor for Measuring PMOS Threshold Voltage Degradation," 2007.
- [32] Y.-M. Kuo, Y.-L. Chang, and S.-C. Chang, "Efficient Boolean characteristic function for timed automatic test pattern generation," *Computer-Aided Design of Integrated Circuits and Systems, IEEE Transactions on*, vol. 28, pp. 417-425, 2009.
- [33] K.-C. Wu and D. Marculescu, "Joint logic restructuring and pin reordering against NBTI-induced performance degradation," in *Proceedings of the Conference on Design, Automation and Test in Europe*, 2009, pp. 75-80.
- [34] F. Oboril and M. B. Tahoori, "Aging-aware design of microprocessor instruction pipelines," *Computer-Aided Design of Integrated Circuits and Systems, IEEE Transactions on*, vol. 33, pp. 704-716, 2014.
- [35] Y. Chen, Y. Xie, Y. Wang, and A. Takach, "Minimizing leakage power in aging-bounded high-level synthesis with design time multi-V<sub>th</sub> assignment," in *Design Automation Conference (ASP-DAC), 2010 15th Asia and South Pacific*, 2010, pp. 689-694.
- [36] M. Denais, C. Parthasarathy, G. Ribes, Y. Rey-Tauriac, N. Revil, A. Bravaix, *et al.*, "On-the-fly characterization of NBTI in ultra-thin gate oxide PMOSFET's," in *Electron Devices Meeting, 2004. IEDM Technical Digest. IEEE International*, 2004, pp. 109-112.
- [37] J. Keane, X. Wang, D. Persaud, and C. H. Kim, "An all-in-one silicon odometer for separately monitoring HCI, BTI, and TDDB," *Solid-State Circuits, IEEE Journal of*, vol. 45, pp. 817-829, 2010.
- [38] E. Karl, P. Singh, D. Blaauw, and D. Sylvester, "Compact in-situ sensors for monitoring negative-bias-temperature-instability effect and oxide degradation," in *Solid-State*

- Circuits Conference, 2008. ISSCC 2008. Digest of Technical Papers. IEEE International, 2008, pp. 410-623.*
- [39] K. K. Kim, W. Wang, and K. Choi, "On-chip aging sensor circuits for reliable nanometer MOSFET digital circuits," *Circuits and Systems II: Express Briefs, IEEE Transactions on*, vol. 57, pp. 798-802, 2010.
  - [40] T.-H. Kim, R. Persaud, and C. H. Kim, "Silicon odometer: An on-chip reliability monitor for measuring frequency degradation of digital circuits," *Solid-State Circuits, IEEE Journal of*, vol. 43, pp. 874-880, 2008.
  - [41] H. K. Alidash, A. Calimera, A. Macii, E. Macii, and M. Poncino, "On-Chip NBTI and PBTI Tracking through an All-Digital Aging Monitor Architecture," in *Integrated Circuit and System Design. Power and Timing Modeling, Optimization and Simulation*, ed: Springer, 2012, pp. 155-165.
  - [42] S. Wang, J. Chen, and M. Tehranipoor, "Representative critical reliability paths for low-cost and accurate on-chip aging evaluation," in *Proceedings of the International Conference on Computer-Aided Design*, 2012, pp. 736-741.
  - [43] H. F. Dadgour and K. Banerjee, "A built-in aging detection and compensation technique for improving reliability of nanoscale CMOS designs," in *Reliability Physics Symposium (IRPS), 2010 IEEE International*, 2010, pp. 822-825.
  - [44] Z. Qi, J. Wang, A. Cabe, S. Wooters, T. Blalock, B. Calhoun, *et al.*, "SRAM-based NBTI/PBTI sensor system design," in *Proceedings of the 47th Design Automation Conference*, 2010, pp. 849-852.
  - [45] KEITHLEY, "Model 4200-BTI-A Ultra-Fast NBTI/PBTI Package," 2015.

- [46] R. A. Ashraf, "Adaptive Architectural Strategies For Resilient Energy-Aware Computing," Doctoral of Philosophy, Department of Electrical and Computer Engineering, University of Central Florida, 2015.
- [47] L. Zhang and R. P. Dick, "Scheduled voltage scaling for increasing lifetime in the presence of NBTI," in *Design Automation Conference, 2009. ASP-DAC 2009. Asia and South Pacific*, 2009, pp. 492-497.
- [48] X. Yang and K. Saluja, "Combating NBTI degradation via gate sizing," in *Quality Electronic Design, 2007. ISQED'07. 8th International Symposium on*, 2007, pp. 47-52.
- [49] J. Chen, S. Wang, and M. Tehranipoor, "Efficient selection and analysis of critical-reliability paths and gates," in *Proceedings of the great lakes symposium on VLSI*, 2012, pp. 45-50.
- [50] D. Sylvester and A. Srivastava, "Computer-aided design for low-power robust computing in nanoscale CMOS," *Proceedings of the IEEE*, vol. 95, pp. 507-529, 2007.
- [51] S. Kothawade, D. M. Ancajas, K. Chakraborty, and S. Roy, "Mitigating NBTI in the physical register file through stress prediction," in *Computer Design (ICCD), 2012 IEEE 30th International Conference on*, 2012, pp. 345-351.
- [52] S. Khan and S. Hamdioui, "Modeling and mitigating NBTI in nanoscale circuits," in *On-Line Testing Symposium (IOLTS), 2011 IEEE 17th International*, 2011, pp. 1-6.
- [53] X. Chen, Y. Wang, H. Yang, Y. Xie, and Y. Cao, "Assessment of Circuit Optimization Techniques Under NBTI," *IEEE Design & Test*, vol. 30, pp. 40-49, 2013.



- [54] F. Firouzi, F. Ye, K. Chakrabarty, and M. B. Tahoori, "Representative critical-path selection for aging-induced delay monitoring," in *Test Conference (ITC), 2013 IEEE International*, 2013, pp. 1-10.
- [55] J. Blome, S. Feng, S. Gupta, and S. Mahlke, "Self-calibrating online wearout detection," in *Proceedings of the 40th Annual IEEE/ACM International Symposium on Microarchitecture*, 2007, pp. 109-122.
- [56] E. Mintarno, J. Skaf, R. Zheng, J. B. Velamala, Y. Cao, S. Boyd, *et al.*, "Self-tuning for maximized lifetime energy-efficiency in the presence of circuit aging," *Computer-Aided Design of Integrated Circuits and Systems, IEEE Transactions on*, vol. 30, pp. 760-773, 2011.
- [57] O. Khan and S. Kundu, "A self-adaptive system architecture to address transistor aging," in *Design, Automation & Test in Europe Conference & Exhibition, 2009. DATE'09.*, 2009, pp. 81-86.
- [58] T.-B. Chan, J. Sartori, P. Gupta, and R. Kumar, "On the efficacy of NBTI mitigation techniques," in *Design, Automation & Test in Europe Conference & Exhibition (DATE), 2011*, 2011, pp. 1-6.
- [59] Z. Qi and M. R. Stan, "NBTI resilient circuits using adaptive body biasing," in *Proceedings of the 18th ACM Great Lakes symposium on VLSI*, 2008, pp. 285-290.
- [60] S. V. Kumar, C. H. Kim, and S. S. Sapatnekar, "Adaptive techniques for overcoming performance degradation due to aging in CMOS circuits," *Very Large Scale Integration (VLSI) Systems, IEEE Transactions on*, vol. 19, pp. 603-614, 2011.

- [61] S. Gupta and S. S. Sapatnekar, "Employing circadian rhythms to enhance power and reliability," *ACM Transactions on Design Automation of Electronic Systems (TODAES)*, vol. 18, p. 38, 2013.
- [62] A. Calimera, E. Macii, and M. Poncino, "NBTI-aware clustered power gating," *ACM Transactions on Design Automation of Electronic Systems (TODAES)*, vol. 16, p. 3, 2010.
- [63] F. Oboril and M. B. Tahoori, "ExtraTime: Modeling and analysis of wearout due to transistor aging at microarchitecture-level," in *Dependable Systems and Networks (DSN), 2012 42nd Annual IEEE/IFIP International Conference on*, 2012, pp. 1-12.
- [64] J. Sun, R. Lysecky, K. Shankar, A. Kodi, A. Louri, and J. Roveda, "Workload assignment considering NBTI degradation in multicore systems," *ACM Journal on Emerging Technologies in Computing Systems (JETC)*, vol. 10, p. 4, 2014.
- [65] X. Chen, Y. Wang, Y. Liang, Y. Xie, and H. Yang, "Run-time technique for simultaneous aging and power optimization in GPGPUs," in *Design Automation Conference (DAC), 2014 51st ACM/EDAC/IEEE*, 2014, pp. 1-6.
- [66] F. Firouzi, S. Kiamehr, and M. B. Tahoori, "Power-aware minimum NBTI vector selection using a linear programming approach," *Computer-Aided Design of Integrated Circuits and Systems, IEEE Transactions on*, vol. 32, pp. 100-110, 2013.
- [67] U. R. Karpuzcu, B. Greskamp, and J. Torrellas, "The BubbleWrap many-core: popping cores for sequential acceleration," in *Microarchitecture, 2009. MICRO-42. 42nd Annual IEEE/ACM International Symposium on*, 2009, pp. 447-458.

- [68] J. Srinivasan, S. V. Adve, P. Bose, and J. A. Rivers, "Exploiting structural duplication for lifetime reliability enhancement," in *ACM SIGARCH Computer Architecture News*, 2005, pp. 520-531.
- [69] R. A. Ashraf, N. Khoshavi, A. Alzahrani, R. F. DeMara, S. Kiamehr, and M. Tahoori, "Area-Energy Tradeoffs of Logic Wear-Leveling for BTI-induced Aging," presented at the ACM International Conference on Computing Frontiers 2016, Italy, 2016.
- [70] D. Ernst, N. S. Kim, S. Das, S. Pant, R. Rao, T. Pham, *et al.*, "Razor: A low-power pipeline based on circuit-level timing speculation," in *Microarchitecture, 2003. MICRO-36. Proceedings. 36th Annual IEEE/ACM International Symposium on*, 2003, pp. 7-18.
- [71] A. Calimera, E. Macii, and M. Poncino, "NBTI-aware power gating for concurrent leakage and aging optimization," in *Proceedings of the 2009 ACM/IEEE international symposium on Low power electronics and design*, 2009, pp. 127-132.
- [72] A. Calimera, E. Macii, and M. Poncino, "NBTI-aware sleep transistor design for reliable power-gating," in *Proceedings of the 19th ACM Great Lakes symposium on VLSI*, 2009, pp. 333-338.
- [73] K.-C. Wu, D. Marculescu, M.-C. Lee, and S.-C. Chang, "Analysis and mitigation of NBTI-induced performance degradation for power-gated circuits," in *Proceedings of the 17th IEEE/ACM international symposium on Low-power electronics and design*, 2011, pp. 139-144.
- [74] L. Liu and H. Mahmoodi, "Evaluation of power gating under transistor aging effect issues in 22nm CMOS technology," in *Mixed Design of Integrated Circuits and Systems (MIXDES), 2010 Proceedings of the 17th International Conference*, 2010, pp. 477-481.

- [75] G. Hoang, R. B. Findler, and R. Joseph, "Exploring circuit timing-aware language and compilation," in *ACM SIGPLAN Notices*, 2011, pp. 345-356.
- [76] X. Bai, C. Visweswariah, and P. N. Strenski, "Uncertainty-aware circuit optimization," in *Proceedings of the 39th annual Design Automation Conference*, 2002, pp. 58-63.
- [77] Y. Lin and M. Zwolinski, "A cost-efficient self-checking register architecture for radiation hardened designs," in *Circuits and Systems (ISCAS), 2014 IEEE International Symposium on*, 2014, pp. 149-152.
- [78] A. Alzahrani. (2016). *CAL Ph.D. Alum*. Available: Retrieved March 28, 2016, from <http://cal.ucf.edu/al-zahrani.html>
- [79] M. B. Taylor, "A landscape of the new dark silicon design regime," *Micro, IEEE*, vol. 33, pp. 8-19, 2013.
- [80] I. Synopsys, "HSPICE User's Manual: Simulation and Analysis," 2010.